

3. SATURATED ZONE RADIONUCLIDE TRANSPORT

If radionuclides are released in the aqueous phase from the repository and migrate through the unsaturated zone as dissolved species or sorbed onto colloids, they will enter the groundwater flow regime in the saturated zone. Released radionuclides would be expected to travel along the groundwater flow paths described in Section 2 (Figure 2-38). The rate of radionuclide transport is a function of key radionuclide transport processes and parameters such as effective porosity, matrix diffusion, hydrodynamic dispersion, and radionuclide sorption (i.e., retardation). The transport of radionuclides as solute is affected by advection, diffusion, and dispersion, and for reactive constituents, sorption. The transport of radionuclides sorbed onto colloids is affected by filtering (where colloids with diameters greater than the pore openings are filtered by the medium) and by attachment-detachment processes. Mixing and dilution of radionuclides in the groundwater affects the concentration of radionuclides released to the environment. This section presents observations and test data that provide the conceptual basis and understanding of radionuclide transport through the saturated zone.

3.1 INTRODUCTION

Processes relevant to the performance of the saturated zone barrier at Yucca Mountain are described conceptually in Figure 3-1. Advection, matrix diffusion, dispersion, and sorption processes occur at different scales within the saturated zone. The effect and importance of these processes differ in the fractured tuff units and the porous alluvium.

In fractured tuffs, advective transport occurs within fractures; therefore, the effective fracture spacing and porosity are important for describing the advective velocity of dissolved constituents. Major flowing fracture zones (termed flowing intervals) are generally spaced on the order of meters to tens of meters apart, while fractures themselves may be more closely spaced and have sub-millimeter apertures. Radionuclides that are transported through the fractures may diffuse into the surrounding matrix or sorb onto the fracture surfaces. If the radionuclides diffuse into the matrix, they may also be sorbed within the matrix of the rock.

In the alluvium, advective transport occurs through the porous matrix. Because the effective porosity of the alluvium is considerably greater than that of the fractured tuff, the transport velocity in the alluvium is greatly reduced in comparison to that of the tuff (even though the specific discharge in the alluvium is about a factor of three greater than that of the tuff; see Section 2.3.7). Radionuclides transported through the porous alluvium can also sorb onto minerals within the alluvium.

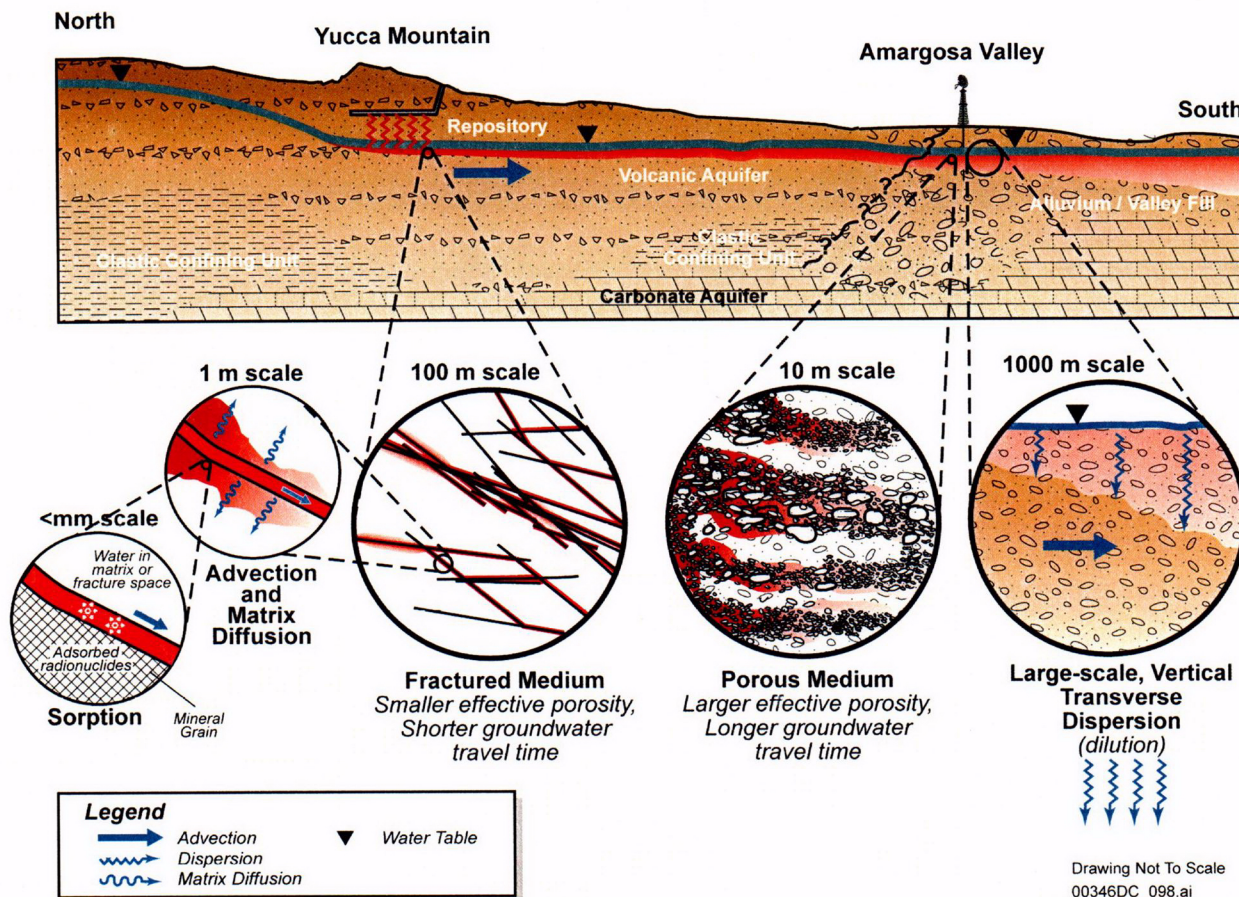


Figure 3-1. Conceptual Model of Radionuclide Transport Processes in the Saturated Zone

In addition to the advective, diffusive, and retardation mechanisms, small-scale heterogeneities in aquifer characteristics, which result in a small-scale variability in advective velocities, can effectively disperse the radionuclides as they migrate through the saturated zone. This dispersive phenomenon tends to allow some radionuclides released at a particular point to migrate either faster than or slower than the average velocity along the groundwater flow trajectory.

Finally, although it is possible for groundwater beneath Yucca Mountain to mix with other groundwater as they flow southward towards Amargosa Valley, it is apparent that the likely flow paths remain constrained over an aquifer width of a few kilometers. At the compliance point, located about 18 km south of Yucca Mountain, the reasonably maximally exposed individual uses well water that is extracted from the aquifer at a rate of $3.7 \times 10^6 \text{ m}^3/\text{year}$ (3,000 acre-ft/year). The hypothetical well is located in the center of the groundwater flow trajectories to maximize the concentration of any dissolved radionuclides that may be contained within the groundwater. The pumping discharge is likely to extract all of the radionuclides in the groundwater at the well location, plus mix with other groundwater that does not contain any radionuclides. The effective concentration in water used by the reasonably maximally exposed individual reflects this mixing process for the purposes of determining the potential dose attributed to these radionuclides.

The processes that affect transport in the tuff and alluvium can be organized and discussed in different ways. For example, all of the processes that might affect transport could be listed and discussed without regard to whether they occur in the fractured tuff or in the alluvium. Alternatively, transport processes for the tuff and alluvium could be discussed separately. The following presentation combines these two approaches. In Section 3.2, processes affecting advective transport of radionuclides for which little retardation is expected by sorption are presented (i.e., advection, matrix diffusion, and dispersion). These processes are presented separately for the fractured tuff (Section 3.2.1) and the alluvium (Section 3.2.2). Processes affecting radionuclide sorption are presented in Section 3.3. Similarly, these processes are presented separately for the fractured tuff (Section 3.3.1) and the alluvium (Section 3.3.2). In Section 3.4, the combined effect of all of these processes is presented in terms of expected radionuclide arrival time profiles (e.g., breakthrough curves), which illustrates the effect of the saturated zone barrier on radionuclide transport.

3.2 ADVECTION, MATRIX DIFFUSION, AND DISPERSION

Advection drives the movement of dissolved constituents in flowing groundwater. The rate of advection is determined by the groundwater velocity, which is controlled by specific discharge and effective porosity. The effective porosity (i.e., the void volume through which the dissolved constituents are likely to flow) is a function of the material properties of the hydrostratigraphic units along the flow paths.

Diffusion of dissolved or colloidal radionuclides into regions of slowly moving groundwater is an important retardation process. Dissolved radionuclides will diffuse from water flowing in the fractures into the matrix, or nonfractured portion of the rocks, as well as from water in pores between rock grains in the alluvium into pore spaces within the rock grains. The radionuclides will eventually diffuse back into the moving groundwater; however, diffusion into and out of the rock matrix and grains will slow the rate of transport.

Hydrodynamic dispersion, the spreading of solutes along a flow path, decreases the concentration of radionuclides. Dispersion occurs because of heterogeneity in flow velocities resulting from heterogeneity of permeability. This heterogeneity can occur at scales ranging from microscopic to the scale of the rock units.

3.2.1 Advection, Diffusion, and Dispersion Processes and Parameters for Fractured Volcanic Tuffs

The advective-diffusive transport properties important to radionuclide transport through the fracture tuffs beneath and downgradient from Yucca Mountain include the fracture (flowing interval) spacing, the effective fracture porosity, matrix diffusion, and hydrodynamic dispersion. The first two of these affect the mean advective velocity, while the second two affect the range of advective transport times through the fractured rock mass.

The transport characteristics of the fractured tuff aquifers in the vicinity of Yucca Mountain generally have been inferred from hydraulic testing in boreholes that penetrate the saturated zone. This general information has been enhanced by hydraulic tests and single- and multiple-well tracer tests at the C-Wells complex (Figure 2-26). Data from the hydraulic and

tracer tests have been supplemented by analyses of ^{14}C to confirm the understanding of advective transport over larger scales relevant to performance of the Yucca Mountain repository.

Results from hydraulic and tracer testing at the C-Wells complex have been used to identify and confirm the conceptualization of flow and transport in the fractured tuff. These results also have been used to derive values for flow and transport modeling parameters. These tests confirm the dual-porosity conceptualization of transport, in which transport takes place in the fracture and matrix porosity of the fractured rock mass. The testing sequence is summarized below, and details important to determining transport characteristics are presented in the appropriate sections.

A series of cross-hole radial converging tracer tests were performed in the Bullfrog-Tram and Prow Pass units at the C-Wells complex (Figure 2-27) using suites of reactive and nonreactive tracers to determine parameters necessary to model advection, dispersion, diffusion, and sorption. Conservative tracer tests conducted at the C-Wells complex include:

- Iodide injection into the combined Bullfrog-Tram interval
- Injection of iodide into the Lower Bullfrog interval
- Injection of 2,6 difluorobenzoic acid into the lower Bullfrog interval
- Injection of 3-carbamoyl-2-pyridone into the Lower Bullfrog interval
- Injection of iodide and 2,4,5 trifluorobenzoic acid into the Prow Pass formation
- Injection of 2,3,4,5 tetrafluorobenzoic acid into the Prow Pass formation
- Injection of pentafluorobenzoic acid into the Lower Bullfrog interval
- Injection of multiple solute and colloid tracers (carboxylate-modified latex microspheres) between boreholes UE-25 c#2 and UE-25 c#3. One test was conducted in the Lower Bullfrog Tuff and another was conducted in the Prow Pass Tuff.

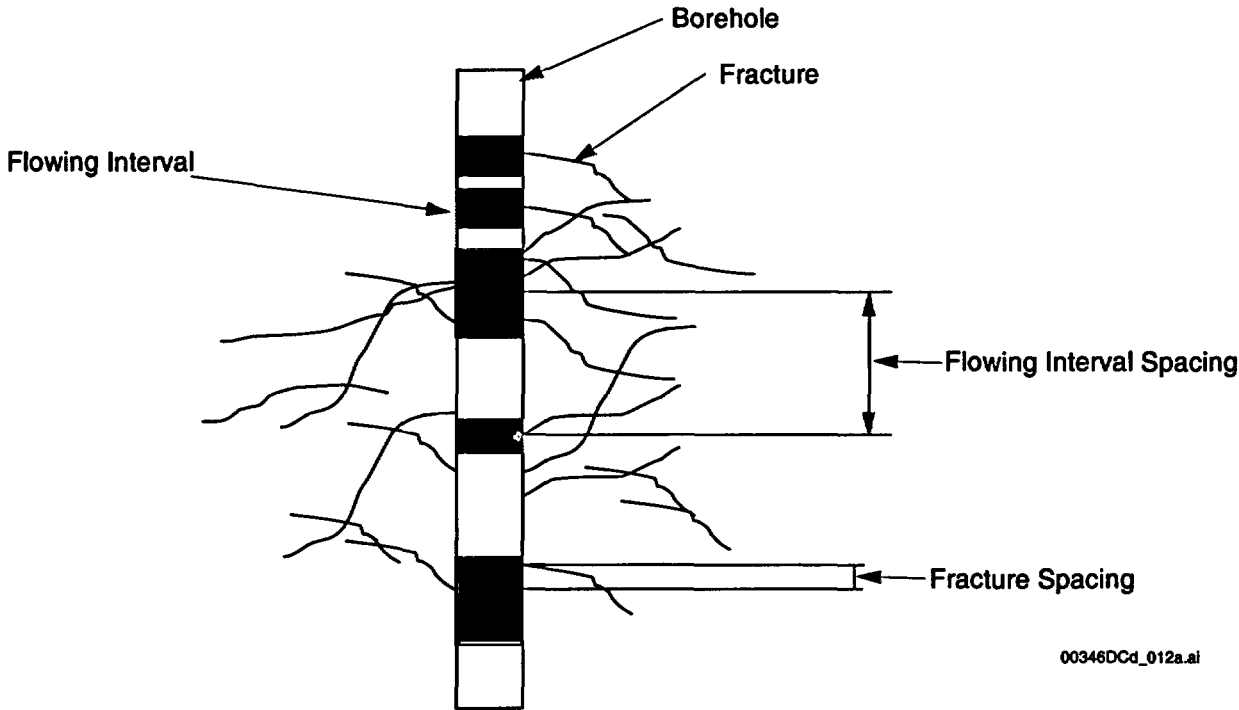
3.2.1.1 Fracture Flowing Interval Spacing

Hydrologic evidence at Yucca Mountain supports the model of fluid flow within fractures in the moderately to densely welded tuffs of the saturated zone (CRWMS M&O 2000a, Section 3.2.2). For example, the bulk hydraulic conductivities measured in the field (which are dominated by fracture flow) tend to be several orders of magnitude higher than hydraulic conductivities of intact (primarily unfractured) tuff core samples measured in the laboratory. Also, there is a positive correlation between fractures identified using acoustic televiewer or borehole television tools and zones of high transmissivity and flow (Erickson and Waddell 1985, Figure 3). This implies that flow occurs primarily through the fracture system, not through the matrix between fractures. Fractures generally are found within the moderately to densely welded tuffs.

Flowing interval spacing (Figure 3-2) is a parameter used in the dual porosity transport model. A flowing interval is defined as a fracture zone that transmits fluid in the saturated zone, as

identified through borehole flow-meter surveys. Flowing interval spacing is distinct from fracture spacing. Typically used in the literature, fracture spacing was not used because field data (e.g., fluid logging and fracture mapping conducted in the C-Wells complex) identify zones (i.e., flowing intervals; Figure 2-27) that contain fluid-conducting fractures, but the data do not distinguish how many or which fractures comprise the flowing interval. The data also indicate that numerous fractures between flowing intervals do not transmit groundwater. Flowing interval spacing is measured between the midpoints of each flowing interval.

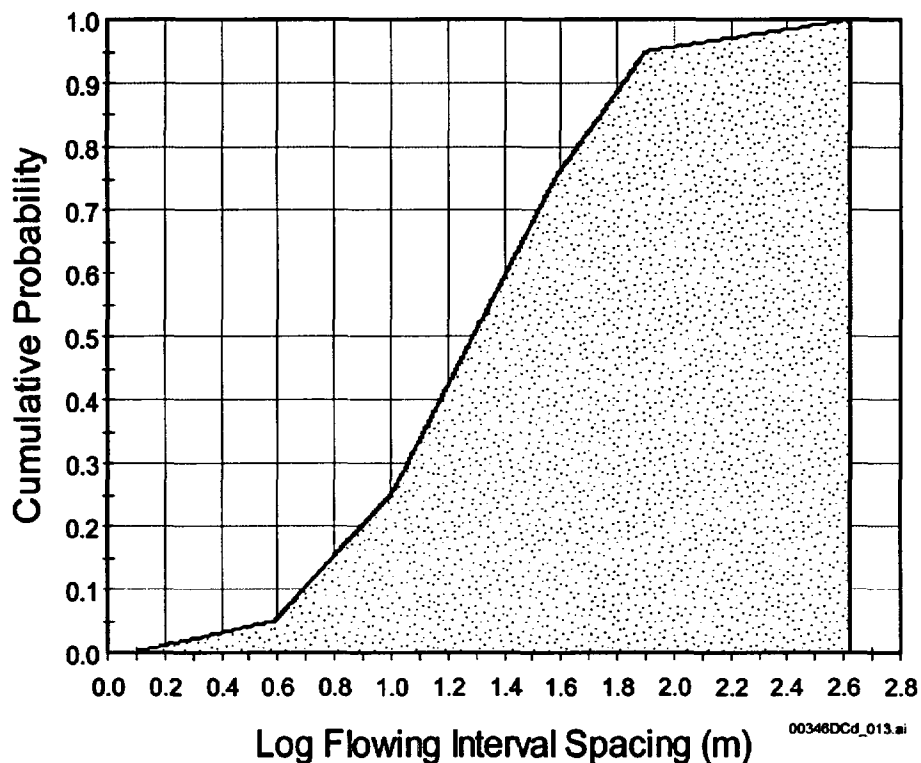
Uncertainty in the flowing interval spacing was included in the transport model. This uncertainty is manifested principally in an effect on matrix diffusion. The larger the spacing between flowing intervals, the less effect matrix diffusion has on delaying radionuclide transport.



Source: BSC 2001d, Figure 1.

Figure 3-2. Conceptual Representation of Flowing Interval Spacing

There is uncertainty associated with the flowing interval spacing due to limited data. The data set used for the analysis consisted of borehole flow-meter survey data. This analysis is described in detail in *Probability Distributions for Flowing Interval Spacing* (BSC 2001d), and it resulted in the distribution for flowing interval spacings indicated in Figure 3-3.



Source: BSC 2003d, Figure 6-12.

Figure 3-3. Cumulative Probability Density Function of Flowing Interval Spacing

3.2.1.2 Fracture Effective Porosity

The flowing interval porosity is defined as the volume of the pore space through which large amounts of groundwater flow occurs, relative to the total volume. The fracture porosity characterizes the effective porosity within flowing intervals rather than within each fracture. The advantage to this definition of fracture porosity is that in situ borehole data may be used to characterize the parameter. The flowing interval porosity may also include the matrix porosity of small matrix blocks within fracture zones. The estimated effective flow porosity values from conservative tracer tests are summarized in Table 3-1.

Table 3-1. Effective Flow Porosity from Conservative Tracer Tests

Tracer Test	Unit	Boreholes (UE-25)	Flow Porosity
Single-Porosity, Partial-Recirculating Solution: 2,4,5 TFBA	Prow Pass	c#3 to c#2	0.05%
Dual-Porosity, Partial-Recirculating Solution: 2,4,5 TFBA	Prow Pass	c#3 to c#2	0.05%
Iodide	Bullfrog-Tram	c#2 to c#3	8.60%
DFBA	Lower Bullfrog	c#2 to c#3	7.2% - 9.9%
Pyridone	Lower Bullfrog	c#1 to c#3	NA

Source: Based on BSC 2003e, Tables 6.3-2 and 6.3-3.

NOTE: TFBA = 2,4,5 trifluorobenzoic acid.

In the Prow Pass, the relatively low flow porosity suggests that advective transport occurs through an interconnected network of fractures, whereas in the Bullfrog-Tram intervals, the relatively large flow porosity suggests a less well-connected fracture network where transport occurs through sections of matrix between fractures. If transport in the Bullfrog-Tram intervals occurred along a tortuous path through a poorly connected network of fractures (which would be much longer than the straight line distance between boreholes), the resulting flow porosities would be much less than 7.2 to 9.9 percent (Table 3-1). In all cases, the data corroborate the concept that flow primarily occurs through fractures.

Table 3-2 summarizes effective flow porosity values derived from two multiple tracer tests, one in the Prow Pass, the other in the Lower Bullfrog. The upper and lower bounds were calculated using mean tracer residence times assuming linear and radial flow, respectively.

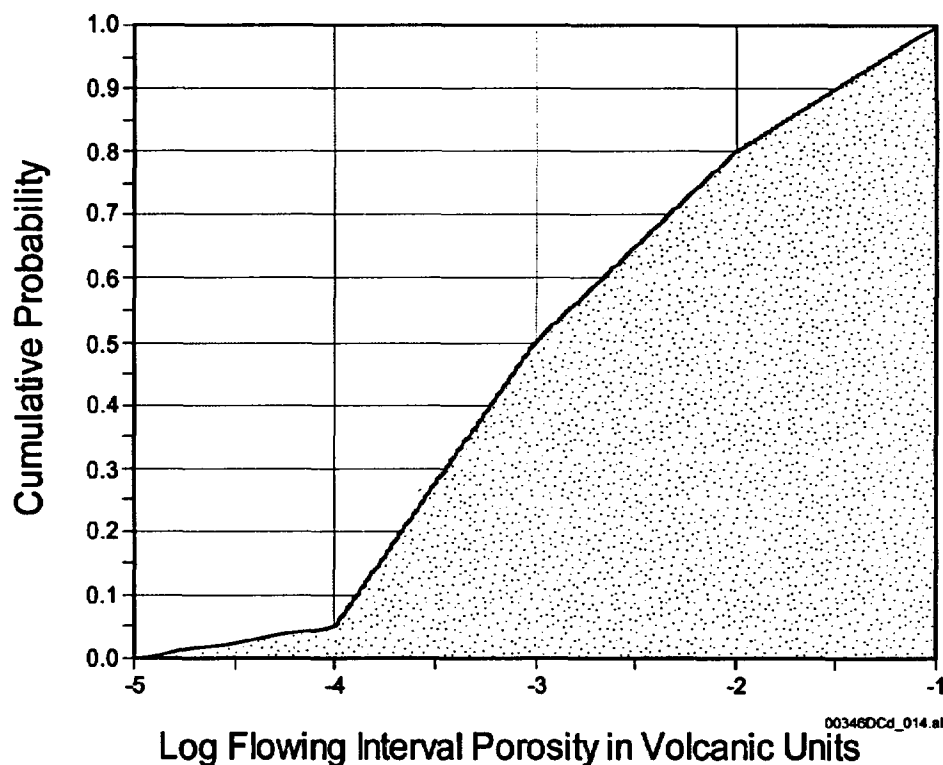
Differences in flow porosity estimates (Tables 3-1 and 3-2) primarily are attributed to different assumptions used in analyses of the tracer tests. Estimates for the lower Bullfrog Tuff are smaller in Table 3-2 than in Table 3-1 because two tracer peaks occurred in the multiple tracer test, and flow was apportioned between these two peaks based on flow surveys and other evidence (BSC 2003e). In contrast, only one peak was observed in each of the conservative tracer tests in the lower Bullfrog Tuff, so all flow was assumed to occur uniformly over the entire tracer test interval, resulting in larger porosity estimates. Flow porosity estimates in the Prow Pass Tuff are smaller in Table 3-1 than in Table 3-2 because a relatively long tracer mean residence time was assumed in the injection borehole in the interpretation of the conservative tracer tests, which resulted in smaller residence times attributed to the aquifer. For the multiple tracer test, a relatively short injection borehole residence time was assumed based on the volume of the packed-off interval and the injection-recirculation rate used in the test. By assuming a smaller residence time in the injection borehole, a longer residence time is attributed to the aquifer, resulting in a larger estimate of flow porosity. Although these alternative interpretive approaches yield a relatively wide range of flow porosity estimates, this wide range reflects the relatively large uncertainties in estimates obtained from tracer tests as a result of the lack of specific knowledge of flow pathways in the aquifer. Details of the analyses are provided in *Saturated Zone In-Situ Testing* (BSC 2003e).

Table 3-2. Flow Porosity Values from Multiple Tracer Tests

Tracer Test	Lower Bound Flow Porosity	Upper Bound Flow Porosity
Prow Pass	0.3%	0.6%
Lower Bullfrog	0.3%	3.1%

Source: BSC 2003e, Table 6.3-10.

Figure 3-4 illustrates the range of likely effective flow porosities derived from C-Wells tests and other site-specific observations. This information was used to define the uncertainty in effective porosity relevant for postclosure performance assessment at Yucca Mountain. The uncertainty distribution (Figure 3-4) is discretized in increments of one order of magnitude, with all of the C-Wells estimates in the range of 0.0001 to 0.1. Seventy-five percent of the values fall between 0.0001 and 0.01, which reflects the judgment that the flow porosity estimates from the C-Wells tests may have been upwardly biased by flow heterogeneity in the fractured tuff. The lower end of the uncertainty range reflects some non-site-specific information on effective flow porosities of fractured rock masses (BSC 2003d).



Source: BSC 2003d, Figure 6-13.

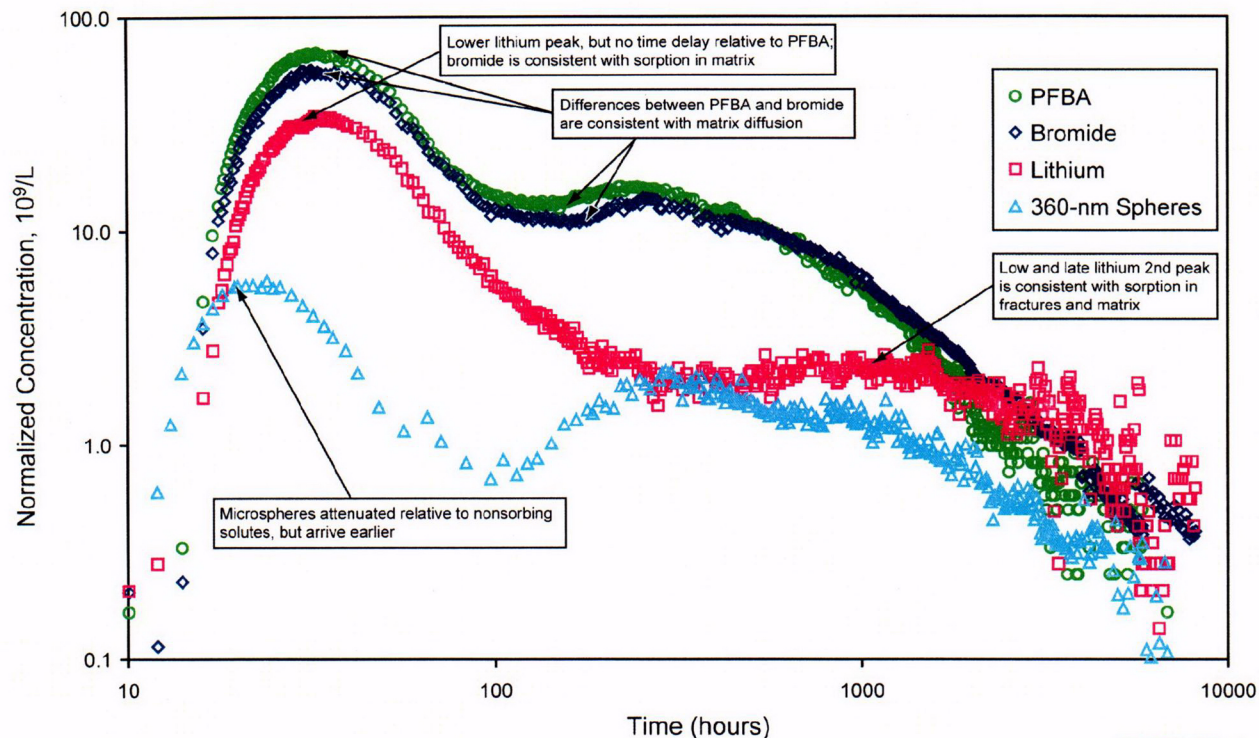
Figure 3-4. Uncertainty in Effective Flow Porosity in Fractured Tuffs at Yucca Mountain

3.2.1.3 Matrix Diffusion

When a molecule (i.e., a dissolved species) travels with groundwater in a fracture, it may migrate by molecular diffusion into the relatively stagnant fluid in the rock matrix, where its velocity effectively becomes zero until Brownian motion carries it back into a fracture. The result of moving into the stagnant matrix is a delay in the arrival time of the molecule at a downgradient location from the time predicted, assuming the molecule had remained in the fracture.

Matrix diffusion occurs in the volcanic rocks in the vicinity of Yucca Mountain (Reimus, Haga et al. 2002; Reimus, Ware et al. 2002). Reimus, Ware et al. (2002) developed an empirical relationship for the effective diffusion coefficient as a function of porosity and permeability measurements based on diffusion cell experiments on rock samples from the Yucca Mountain area. Diffusing species were ^{99}Tc (as TcO_4), ^{14}C (as HCO_3), and tritiated water. Rock samples were taken from the vicinity of Yucca Mountain, Pahute Mesa, and the Nevada Test Site (Area 25). Reimus, Haga et al. (2002) found that differences in rock type account for the largest variability in effective diffusion coefficients, rather than variability among diffusing species, size, and charge.

In the field, cross-hole tracer tests that demonstrate the effect of matrix diffusion have been conducted (BSC 2001e, Section 6). The C-Wells reactive tracer test (BSC 2003e; CRWMS M&O 2000a, Section 3.1.3.2), demonstrated that observed tracer breakthrough is explained by models incorporating matrix diffusion (Figure 3-5).

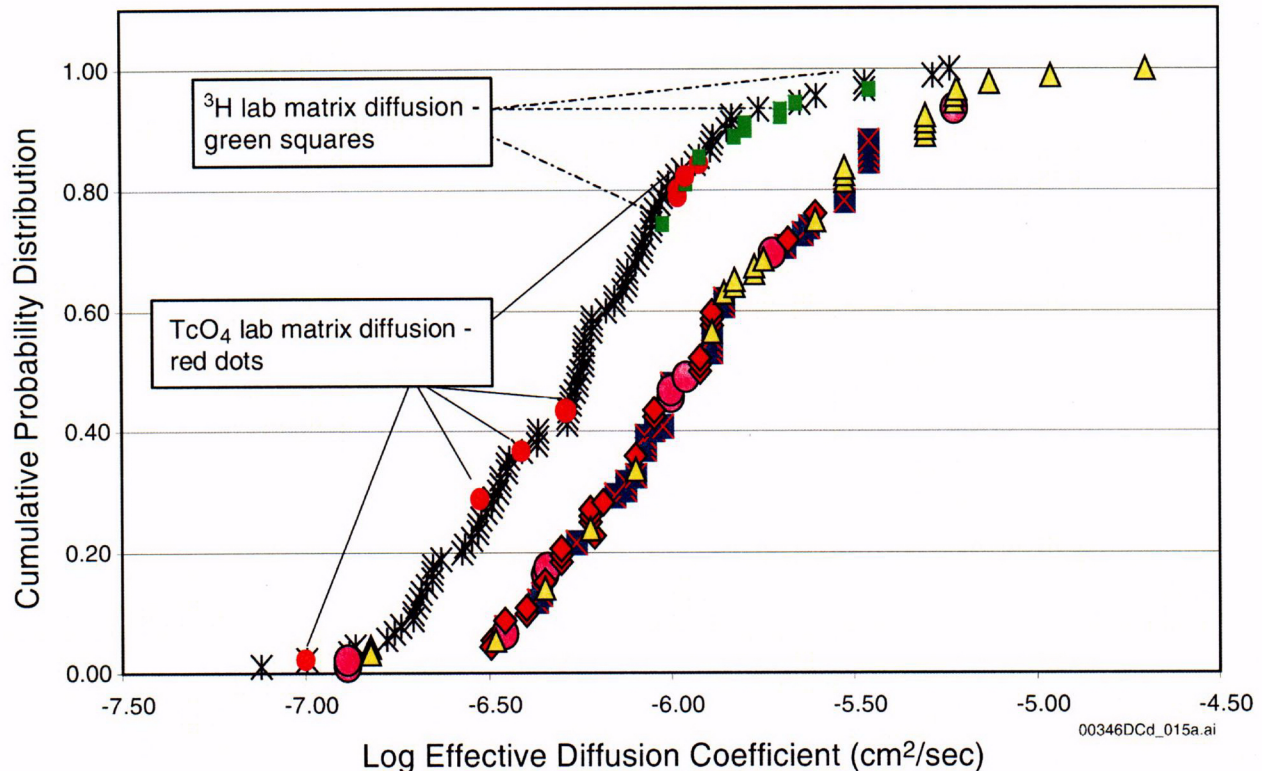


Source: BSC 2001e, Figures 6.3-21 and 6.3-22.

NOTE: Tracer recoveries were about 69 percent for pentafluorobenzoic acid (PFBA), 69 percent for bromide, 39 percent for lithium, and 15 percent for microspheres. Concentrations are normalized to mass injected; both axes are log scale.

Figure 3-5. Normalized Tracer Responses in the Bullfrog Tuff Multiple-Tracer Tests

Laboratory experiments and field tests at Yucca Mountain have demonstrated the validity of matrix diffusion, and they provide a basis for quantifying the effect of matrix diffusion on radionuclide migration through the moderately and densely welded tuffs of the saturated zone. The cumulative distribution of the matrix diffusion coefficient applicable to Yucca Mountain tuffs is illustrated in Figure 3-6.



Source: BSC 2003d, Figure 6-14.

NOTE: The left curve represents effective diffusion coefficient values derived using a linear regression relationship based on porosity and permeability values and diffusion cell results (Reimus, Ware et al. 2002, p. 2.25). Included in the plot are laboratory measurements of effective diffusion coefficient from Triay (1993) and Rundberg et al. (1987) to demonstrate the reasonableness of the derived effective diffusion coefficient values. The right curve represents laboratory and field-derived estimates. Triangles: ^{14}C laboratory values; Squares: tritium laboratory values; Diamonds: TcO_4 laboratory values; Circles: Br^- and pentafluorobenzoic acid field values presented in Reimus, Ware et al. (2002) and *Saturated Zone In-Situ Testing* (BSC 2003e).

Figure 3-6. Matrix Diffusion Coefficients Applicable to Fractured Tuffs at Yucca Mountain

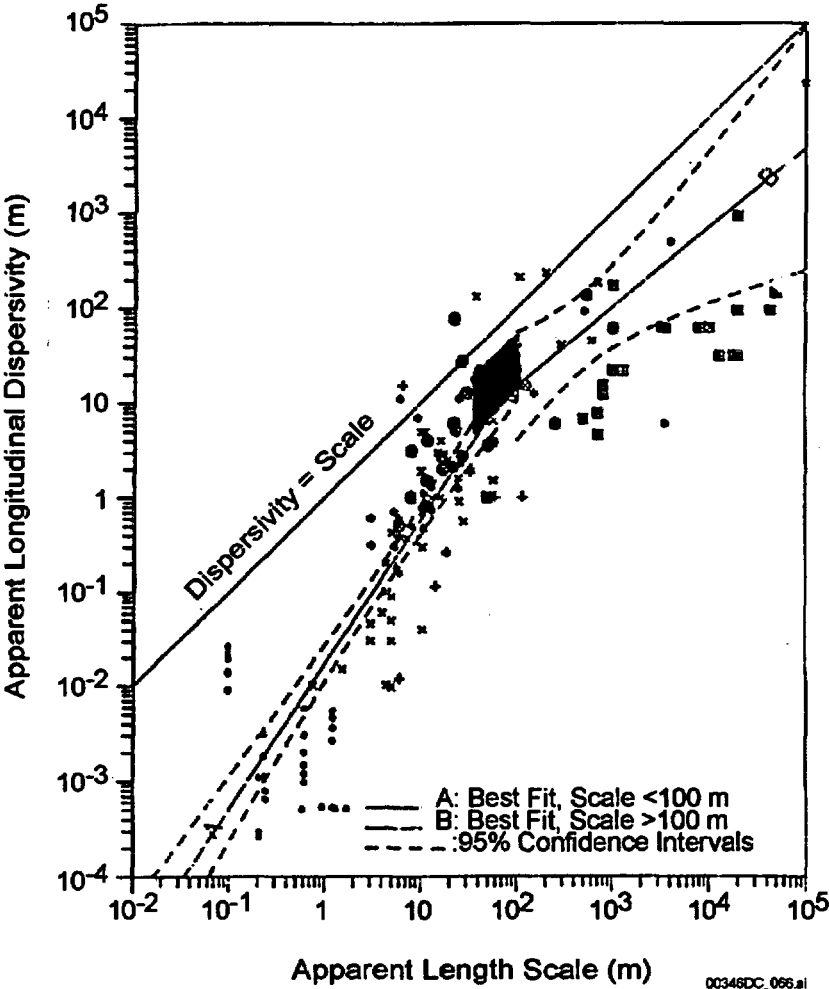
3.2.1.4 Hydrodynamic Dispersion

Dispersive processes can occur at a range of scales and at directions longitudinal and transverse to the average groundwater flow direction. Longitudinal dispersion is a function of several factors including the relative concentrations of the solute, the flow field, and the rock properties. An important component of dispersion is dispersivity, a coarse measure of the solute (mechanical) spreading properties of the rock. Longitudinal dispersivity will be important only at the leading edge of the advancing plume, while transverse dispersivity (horizontal transverse and vertical transverse) affects the width of the plume but not repository performance.

Dispersion is caused by heterogeneities at scales ranging from individual pore spaces to the thickness of individual strata and the length of structural features such as faults. The spreading and dilution of radionuclides that results from these heterogeneities could be important to performance of the repository. Although heterogeneities at the scale of kilometers are represented explicitly in the site-scale saturated zone flow and transport model, dispersion at

smaller scales is characterized using an anisotropic dispersion coefficient tensor consisting of a three-dimensional set of dispersivity values: longitudinal, horizontal-transverse, and vertical-transverse.

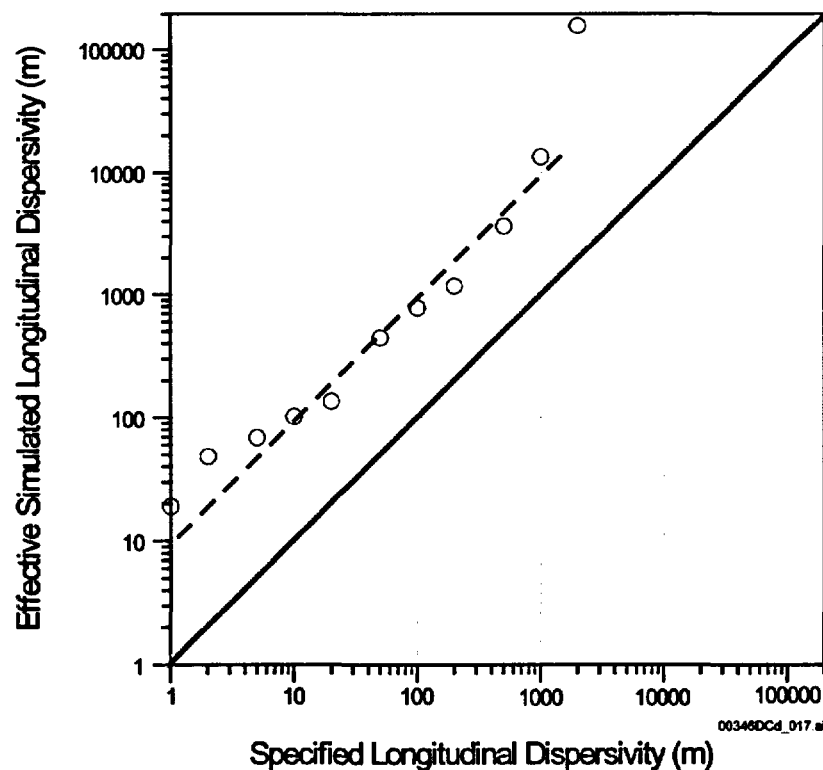
Transport field studies addressing dispersion have been conducted at length scales from meters to kilometers. Figure 3-7 shows estimated dispersivity as a function of length scale. Dispersivity increases as a function of observation scale, which is attributed mainly to mixing as more heterogeneities are encountered by flow at larger scales (Gelhar et al. 1992). Dispersivity values determined for the C-Wells reactive tracer experiment (CRWMS M&O 2000a, Section 3.1.3.2) illustrate a trend toward larger dispersion coefficients for transport over longer distances (Figure 3-7, black diamond).



Source: BSC 2001e, Figure 100.

Figure 3-7. Dispersivity as a Function of Length Scale

Dispersion on the local scale (tens to hundreds of meters) has been specified through simulation of saturated zone transport at Yucca Mountain using a random-walk displacement algorithm. In addition, the spatial distribution of hydrogeologic units with contrasting permeabilities within the model imparts additional dispersion at the scale of kilometers to the simulated transport of particles as flow paths diverge during transport. The effective longitudinal dispersivity due to both processes may be considerably larger than the specified value due to the additive effects of these two processes. Effective longitudinal dispersivity has been analyzed for a range of values of specified longitudinal dispersivity to evaluate the magnitude of this effect. The results of this analysis (BSC 2003d) indicate that the effective simulated longitudinal dispersivity is about one order of magnitude higher than the specified longitudinal dispersivity (Figure 3-8). To account for this numerical effect, the dispersivity used in the model was reduced by an order of magnitude to allow the effective modeled diffusion to be equivalent to the observed dispersivity distribution (Figure 3-8). Because all of the radionuclide mass is captured in the representative volume, transverse vertical and horizontal dispersivity are not pertinent to modeling total system performance assessment for the license application.



Source: BSC 2003d, Figure 6-18.

NOTE: Solid line: effective longitudinal dispersivity equals specified longitudinal dispersivity (i.e., no added effect).
Open circles: calculated effective longitudinal dispersivity. Dashed line: linear fit to the calculated values.

Figure 3-8. Effective Modeled Dispersivity versus Specified Dispersivities using the Site-Scale Radionuclide Transport Model

3.2.2 Advection, Diffusion, and Dispersion Processes and Parameters for Alluvium

Due to the porous nature of the alluvial material, fluid flow in the alluvium is well represented using a porous continuum conceptual model. As a result, the principal transport characteristic of the alluvium relevant to nonsorbing radionuclide migration is the effective porosity.

3.2.2.1 Effective Porosity of the Alluvium

A range of effective porosities for alluvial materials has been presented in the literature (summarized by BSC 2003d). To supplement this distribution, site-specific testing has been performed in single-well tracer tests at the Alluvial Testing Complex. A site-specific value of 0.10 (10 percent) was determined for effective porosity from boreholes NC-EWDP-19D1 based on a single-well pumping test (BSC 2003e). Other total porosity values from the same borehole, based on gravimeter surveys, were used in developing the upper bound of effective porosity in the alluvium uncertainty distribution.

Single-well hydraulic testing of saturated alluvium was conducted in borehole NC-EWDP-19D1 between July 2000 and November 2000. In January 2002, two cross-hole hydraulic tests were performed where NC-EWDP-19D1 was pumped and NC-EWDP-19IM1 and NC-EWDP-19IM2 were used for monitoring.

The total porosity of the alluvium was determined to be about 33 percent from analysis of grain size distributions. An estimate of total porosity using the storage coefficient from the cross-hole hydraulic test, the thickness of the tested interval, and the barometric efficiency of the formation was determined to be 40 percent. These values represent upper bounds of possible porosities that need to be adjusted to account for the effective porosity through which water and any radionuclides are likely to be transported.

In addition, three single-well injection-withdrawal tracer tests were conducted in boreholes NC-EWDP-19D1 between December 2000 and April 2001. In each tracer test, two nonsorbing solute tracers with different diffusion coefficients were simultaneously injected (a halide and a fluorobenzoic acid dissolved in the same solution). Three conceptual models of transport (Figure 3-9) were considered for the saturated valley-fill deposits south of Yucca Mountain:

- The first model (Figure 3-9a) assumes purely advective transport through a porous medium with no diffusive mass transfer into the grains of the medium or between advective and nonadvective regions of the aquifer. This model does not necessarily imply a homogeneous flow field, but it does preclude systems with alternating layers of relatively narrow thickness, considerable differences in permeability, or both. Such a conceptual model might be valid in a sandy aquifer with grains of relatively low porosity.
- The second model (Figure 3-9b) is similar to the first except that it includes diffusive mass transfer into the grains of the porous medium. The grains are internally porous, but the porosity is not well connected over the scale of the grains; therefore, the grains transmit negligible flow.

- The third model (Figure 3-9c) includes diffusive mass transfer between advective and nonadvective layers in the aquifer. In this model, the flow system alternates between high and low conductivity layers, a simplified representation that is consistent with some depositional scenarios. Diffusive mass transfer occurs only between the two layers, not into grains within the layers. However, one variation of this model is to include diffusion into grains in the advective and nonadvective layers. This variation is essentially a combination of the second and third conceptual models, with an additional level of complexity allowing for diffusion in the nonadvective layer into the inter- and intragranular pore spaces.

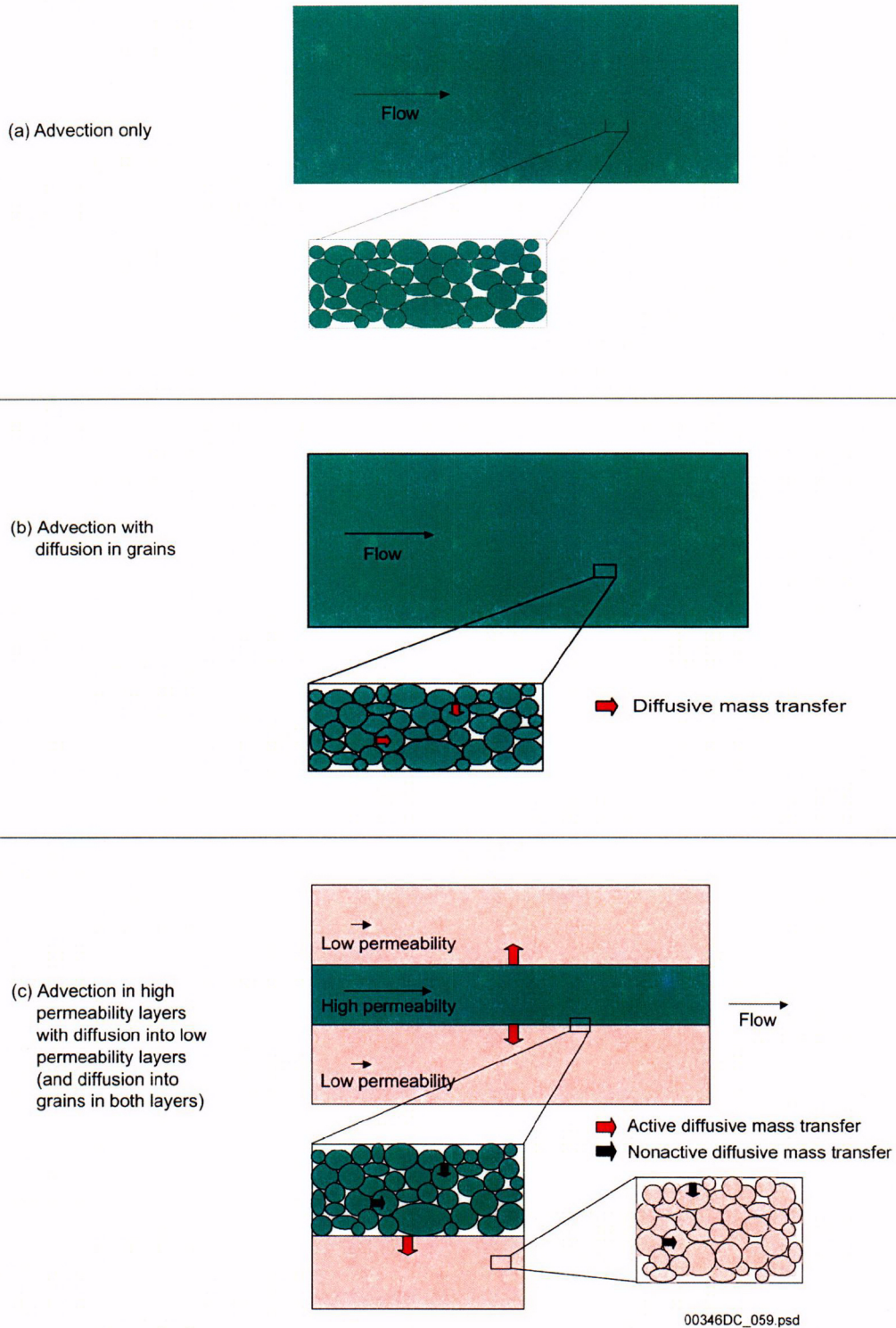
An example of the tracer response, showing nearly identical responses of the paired tracers, is presented in Figure 2-31. The response of the paired tracers with different diffusion coefficients are the same, implying that the conceptual model of a single porosity medium (i.e., the first model, Figure 3-9a) is valid.

Four methods were used to estimate the ambient groundwater velocity from the differences in tracer breakthrough for the various drift periods during the single-well tracer tests. These four methods include the peak arrival, late arrival, and two mean arrival methods. The specific discharge and seepage velocity estimates for three assumed flow porosities are summarized in Table 2-7. Estimates of specific discharge range from 1.2 to 9.4 m/year, which falls within the range of specific discharges derived from the site-scale flow model. Flow porosity (0.10) and longitudinal dispersivity (5 m) estimates were calculated using a linked-analytical-solution method.

Based on these observations and literature surveys, a range of effective porosities is possible for the alluvium. Figure 3-10 illustrates possible distributions, and Figure 3-11 is the effective porosity distribution used in the model. The actual distribution (Figure 3-11) primarily is based on the distribution proposed by Bedinger et al. (1989), truncated at an upper value of 0.3 because 0.29 was the largest value of total porosity measured by borehole gravimetry in NC-EWDP-19D1. Details of the selection of this distribution are provided in Appendix H, Section H.4.2.

3.2.2.2 Alluvium Diffusion

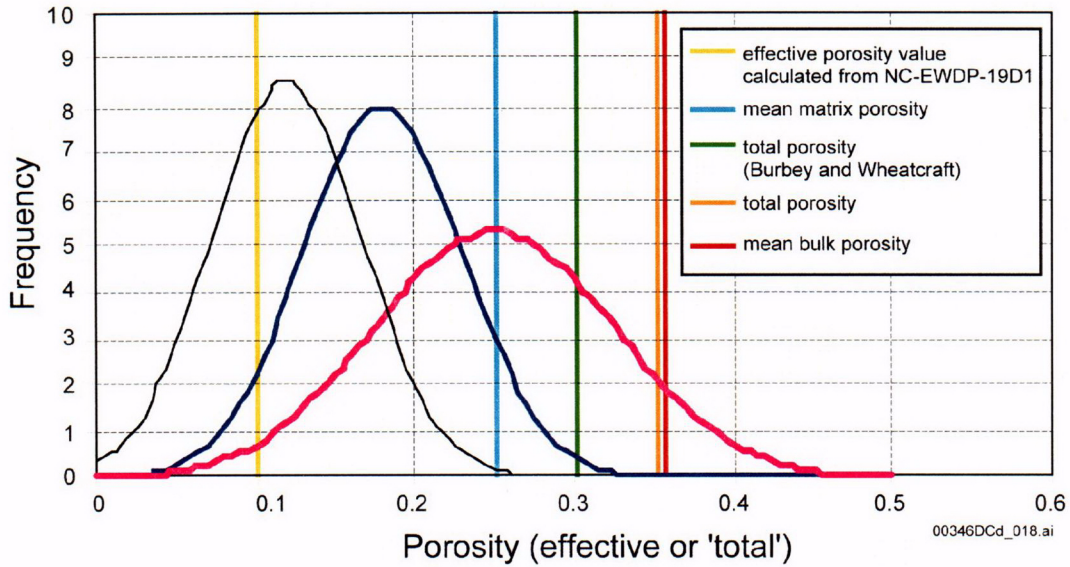
There was virtually no difference in the normalized responses of the halide and fluorobenzoic acid tracers in the three single-well tracer tests conducted in NC-EWDP-19D1, suggesting that a single-porosity conceptual model is appropriate for modeling radionuclide transport of the scale of the test in the saturated alluvium south of Yucca Mountain (BSC 2003e). Further evidence for a single-porosity flow and transport system was provided by the lack of an increase in tracer concentrations after flow interruptions during the tailing portions of the tracer responses in two of the tests. This lack of increase in tracer concentrations indicates a lack of diffusive mass transfer between flowing and stagnant water in the flow system. As a result of these observations, diffusion was not considered in transport in the alluvium.



Source: BSC 2003e, Figure 6.5-1.

NOTES: Red arrows in (c) indicate diffusive mass transfer options that were exercised in this scientific analysis, and black arrows indicate options that were not exercised.

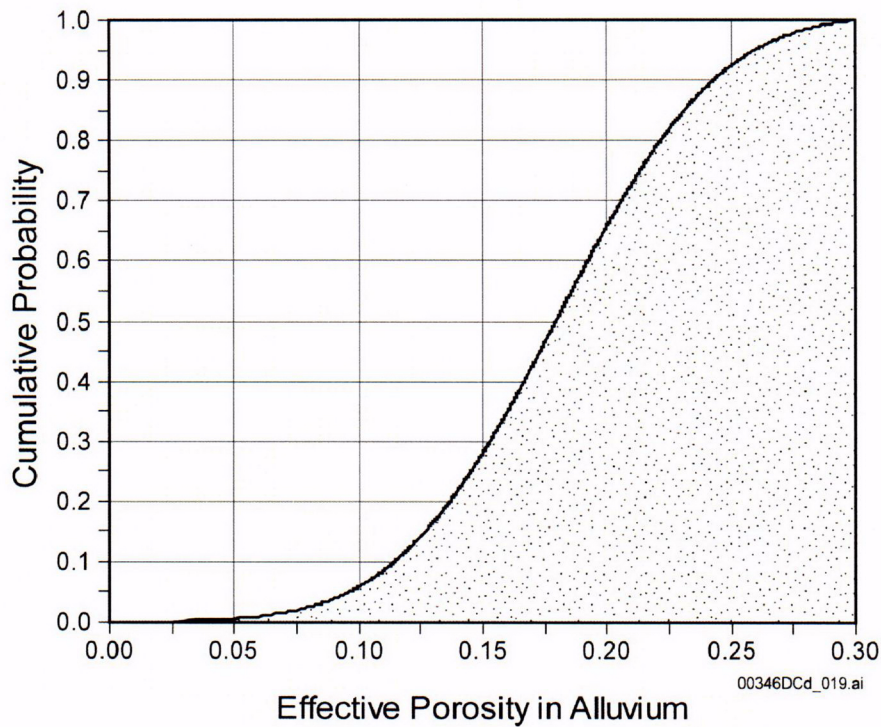
Figure 3-9. Alternative Conceptual Models of Transport in Valley-Fill Deposits



Source: BSC 2003d, Figure 6-8.

NOTE: Solid black distribution is MO0003SZFWTEEP.000; the solid blue distribution is MO0105HCONEPOR.000; the solid pink distribution is MO0003SZFWTEEP.000. All data are from *Regional Groundwater Flow and Tritium Transport Modeling and Risk Assessment of the Underground Test Area, Nevada Test Site, Nevada* (DOE 1997) except for total porosity, which is from Burbey and Wheatcraft (1986).

Figure 3-10. Range of Effective Porosities for Alluvial Materials



Source: BSC 2003d, Figure 6-9.

Figure 3-11. Effective Porosity Distribution used in Yucca Mountain Transport Model

3.2.2.3 Alluvium Dispersivity

Dispersivity in the alluvium has not been measured in the field. However, several column tracer experiments were conducted using groundwater and alluvium from borehole NC-EWDP-19D1 and a sorbing tracer (lithium bromide). Dispersivity values from these experiments ranged from 1.8 to 5.4 cm (BSC 2003e). These dispersivity values are consistent with the scale of the column experiments. However, these values are not appropriate for larger scale simulations because the parameter is scale dependent. A common scale-dependent dispersivity for fractured tuff and alluvium has been used in numerical models of transport at Yucca Mountain (Figure 3-7; see also BSC 2001e).

3.2.3 Corroboration of Tuff and Alluvial Advective Transport Representations Using Carbon Isotope Information

Although the advective transport properties are acceptably constrained by in situ observations from boreholes, these observations are limited by the scale of time and space over which the tests were conducted. The scale of the C-Wells and Alluvial Testing Complex are tens of meters and days to months; however, transport processes relevant to repository performance occurs over scales of kilometers and thousands of years.

One of the few methods to investigate transport processes over the spatial and temporal scale of interest to repository performance is the use of naturally occurring radioisotopes such as ^{14}C . The following discussion summarizes observations of carbon isotopes used to substantiate the properties developed at smaller scales.

3.2.3.1 ^{14}C Background

The radioactive decay of ^{14}C , with a half-life of 5,730 years, forms the basis for radiocarbon dating. The ^{14}C age of a sample is calculated as

$$t = (-1/\lambda) \ln (^{14}\text{A}/^{14}\text{A}_0) \quad (\text{Eq. 3-1})$$

where t is the mean groundwater age (years), λ is the radioactive decay constant ($1.21 \times 10^{-4} \text{ yr}^{-1}$), ^{14}A is the measured ^{14}C activity, and $^{14}\text{A}_0$ is the assumed initial activity. ^{14}C ages typically are expressed in percent modern carbon (pmc). A ^{14}C activity of 100 pmc is taken as the ^{14}C activity of the atmosphere in the year 1890, before natural ^{14}C in the atmosphere was diluted by large amounts of ^{14}C -free carbon dioxide gas from the burning of fossil fuel.

Theoretically, the activity of ^{14}C in a groundwater sample reflects the time when the water was recharged. Unfortunately, precipitation generally has low carbon concentrations and has a high affinity for dissolution of solid phases in the soil zone, unsaturated zone, and saturated zone. In particular, in the transition from precipitation compositions to groundwater compositions, the concentration of combined bicarbonate and carbonate in the water commonly increases by orders of magnitude (Langmuir 1997, Table 8.7; Meijer 2002). Because bicarbonate is the principal ^{14}C -containing species in most groundwater, the source of this additional bicarbonate can affect the apparent "age" calculated from the ^{14}C . If the source of carbon primarily is decaying plant material in an active soil zone, the calculated age for the water sample should be close to the true age. In contrast, if the source of bicarbonate is the dissolution of old (i.e., older than 10^4 years)

calcite with low ^{14}C activity or the oxidation of old organic material, then the calculated age for the sample will be over estimated (older than expected).

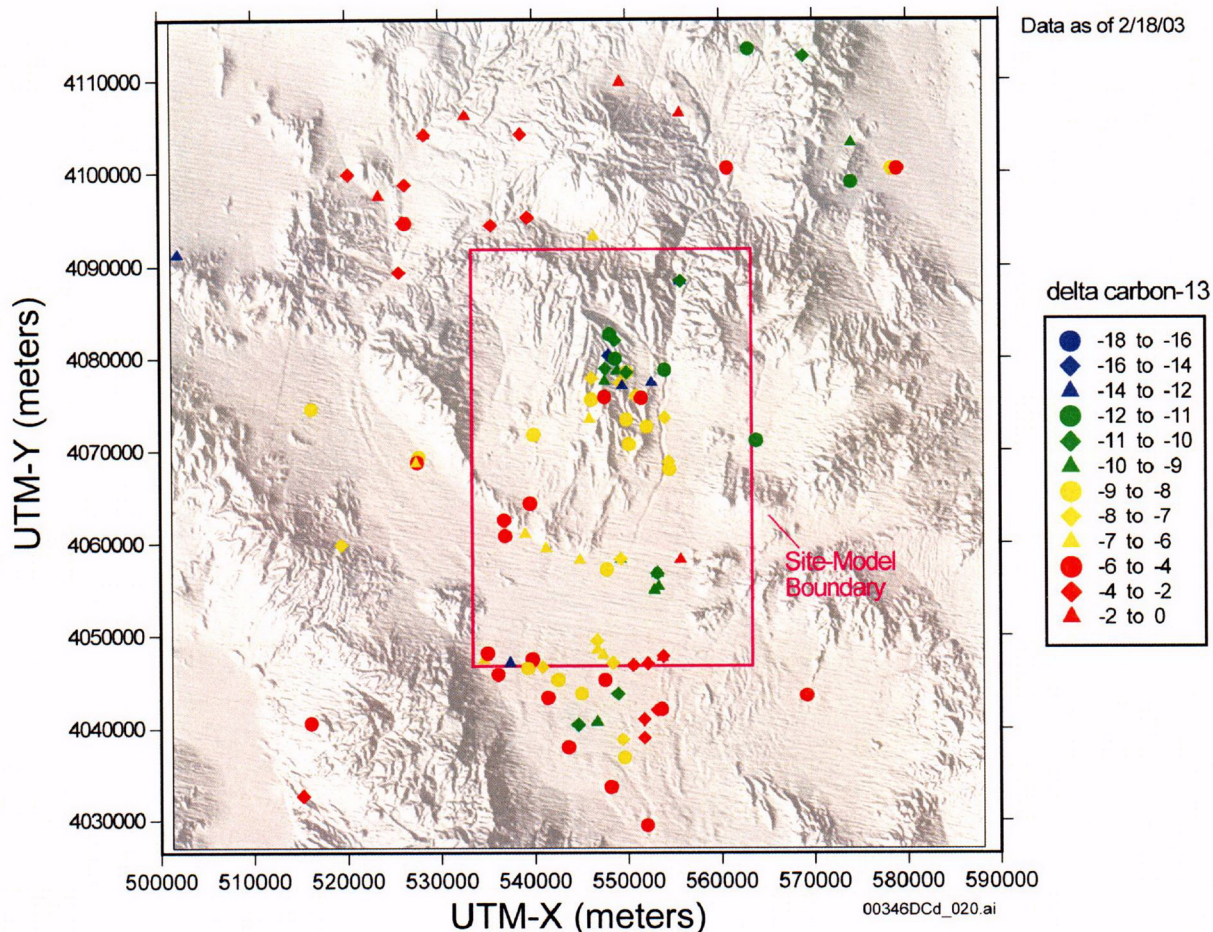
A useful measure of the source of carbon in a water sample is the $\delta^{13}\text{C}$ value of the sample because this value is different for organic materials and calcites. The $\delta^{13}\text{C}$ value, in units of per mil, is defined as

$$\delta^{13}\text{C} = \left[\frac{(^{13}\text{C}/^{12}\text{C})_{\text{sample}}}{(^{13}\text{C}/^{12}\text{C})_{\text{standard}}} - 1 \right] \times 1000 \quad (\text{Eq. 3-2})$$

The $\delta^{13}\text{C}$ values of carbon species typical of the soil waters in arid environments range from -25 to -13/‰ (Forester et al. 1999, p. 36). At Yucca Mountain, pedogenic carbonate minerals have $\delta^{13}\text{C}$ values generally between -8 and -4/‰, although early formed calcites are also present that have $\delta^{13}\text{C}$ values greater than 0/‰ (Forester et al. 1999, Figure 16; Whelan et al. 1998, Figure 5). Paleozoic carbonate rocks typically have $\delta^{13}\text{C}$ values close to 0/‰ (Forester et al. 1999, Figure 16; Whelan et al. 1998, Figure 5).

3.2.3.2 $\delta^{13}\text{C}$ Observations in Groundwater in the Vicinity of Yucca Mountain

The areal distribution of $\delta^{13}\text{C}$ values is shown in Figure 3-12. Groundwater in the northernmost part of Yucca Mountain generally is lighter in $\delta^{13}\text{C}$ than groundwater found toward the central and southern parts of the mountain. North of Yucca Mountain, groundwater $\delta^{13}\text{C}$ values generally are heavier than those found at Yucca Mountain. Overall, the $\delta^{13}\text{C}$ values of groundwater in Nye County Early Warning Drilling Program boreholes at the southern edge of Crater Flat increase to the west, reflecting the increasing component of groundwater from carbonate rocks with $\delta^{13}\text{C}$ values around zero. Groundwater $\delta^{13}\text{C}$ values near Fortymile Wash generally are lower than the $\delta^{13}\text{C}$ values toward the western and eastern parts of the Amargosa Desert, where groundwater $\delta^{13}\text{C}$ values reflect the proximity to carbonate rocks of the southern Funeral Mountains and discharge from the carbonate aquifer across the Gravity Fault, respectively.

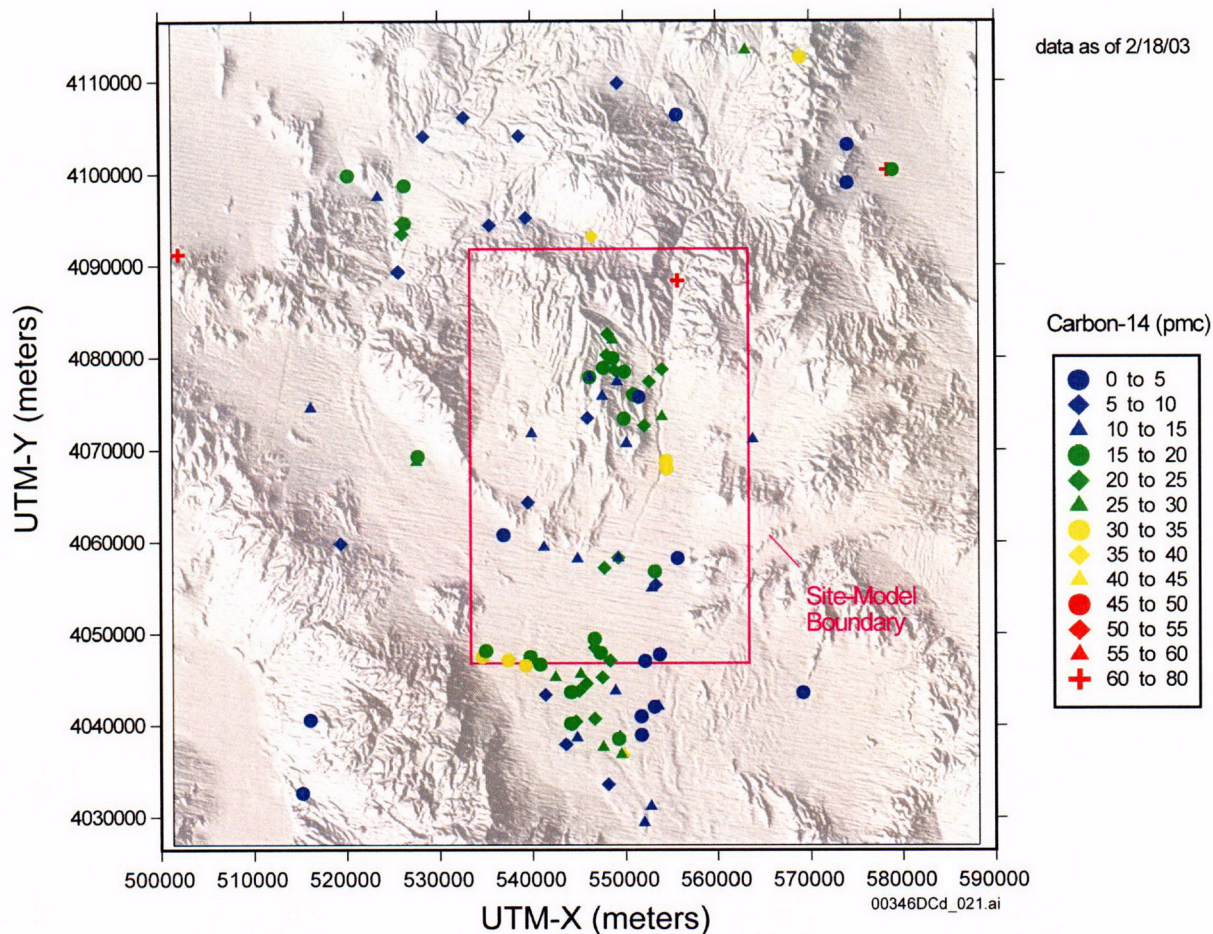


Source: BSC 2003f, Figure 27.

Figure 3-12. Areal Distribution of $\delta^{13}\text{C}$ in Groundwater

3.2.3.3 ^{14}C Observations in Groundwater in the Vicinity of Yucca Mountain

The areal distribution of ^{14}C activity is shown in Figure 3-13. Groundwater at the eastern edge of Crater Flat near Solitario Canyon has some of the lowest ^{14}C activities of groundwater in the map area. Groundwater at several Nye County boreholes in the Yucca Mountain-South grouping, to the south of borehole USW VH-1, has similar ^{14}C activities. The groundwater at boreholes NC-EWDP-2D, NC-EWDP-19P, and some zones in NC-EWDP-19D have a ^{14}C activities of 20 pmc or more, similar to the ^{14}C activities of groundwater in Dune Wash and Fortymile Wash. Groundwater near Fortymile Wash has ^{14}C activities that range from about 76 pmc near the northern boundary of the model area to values under 20 pmc near the southern boundary of the model area. South of the site-model boundary, groundwater ^{14}C activities near Fortymile Wash range from 10 to 40 pmc.

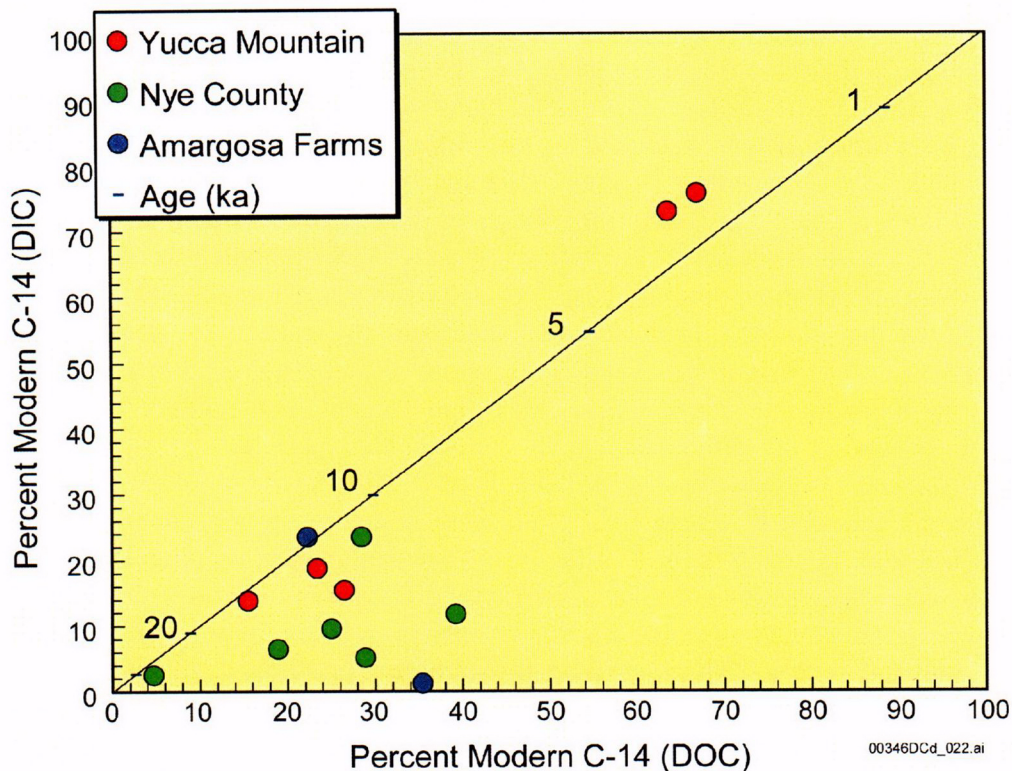


Source: BSC 2003f, Figure 28.

Figure 3-13. ^{14}C Activities in Groundwater

The above observations are based on measurements of dissolved inorganic carbon isotopes. Because the interpretation of such measurements has considerable uncertainty due to varied water-rock interactions that can affect the measured isotope ratios, measurements of dissolved organic carbon content also were made. Carbon isotopes of dissolved organic carbon provide a means independent of dissolved inorganic carbon useful for making age corrections to determine travel times of groundwater in aquifers. Groundwater ages can be calculated directly from dissolved organic carbon ^{14}C values if the ^{14}C of the groundwater in the recharge area is known. Ages calculated from dissolved organic carbon ^{14}C are maximum ages because organic aquifer material would contain no ^{14}C (except for newly drilled boreholes that can contain modern dissolved organic carbon).

Measurements of dissolved inorganic carbon and dissolved organic carbon were made on 13 samples of groundwater from the Yucca Mountain area. Figure 3-14 shows the correlation between ages determined from the two forms of carbon. Most ages based on dissolved inorganic carbon were greater than 12,000 years. The dissolved organic carbon ages generally were younger, but ranged from 8,000 to 16,000 years. The youngest ages were for water samples from upper Fortymile Canyon; these ages showed a slight reverse discordance (i.e., the dissolved inorganic carbon ages were slightly younger than dissolved organic carbon ages).



Source: Peters 2003, Slide 36 of 68.

Note: The numbers on the diagonal line are groundwater ages in thousands of years, calculated assuming $^{14}\text{A}_0$ is 100 pmc. DOC = dissolved organic carbon; DIC = dissolved inorganic carbon; ka = thousand years.

Figure 3-14. Correlation Between Observed Dissolved Organic and Inorganic ^{14}C Ages in Groundwater

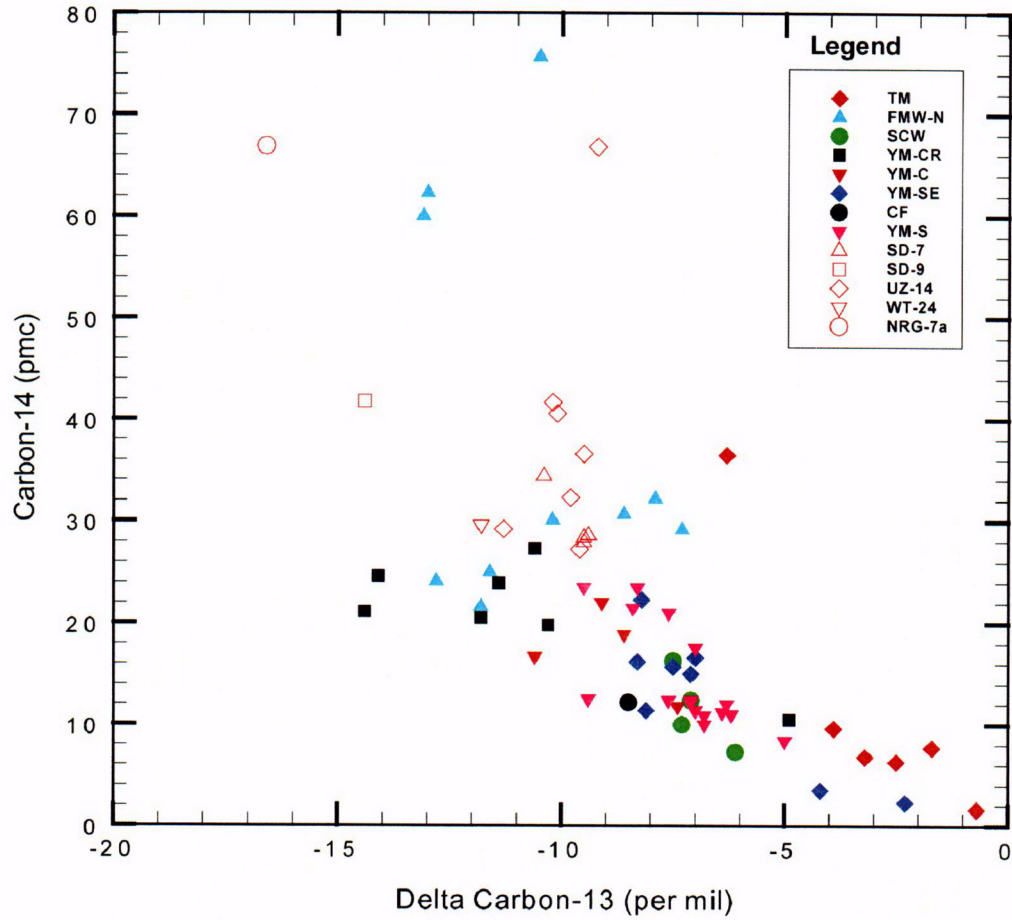
3.2.3.4 Interpretation of Carbon Isotope Data

The measured activity of ^{14}C indicates that most groundwater contains less than 30 pmc, with a few exceptions in northern Fortymile Wash. Trends of decreasing ^{14}C along potential flow paths south of the repository are not evident from most of the data. The carbon (principally bicarbonate) in groundwater is readily modified through reactions with aquifer rock along the flow path. Therefore, it is necessary to evaluate potential sources of carbon in the groundwater before using ^{14}C data to evaluate flow paths or residence times.

Although carbon isotopes were not used to evaluate flow paths, ^{14}C data from groundwater along the potential flow paths was used to infer relative advective transport times. The measured ^{14}C activities were corrected to account for decreases in ^{14}C activity that result from water-rock interactions and the mixing of groundwater (identified by mixing and chemical reaction models; see Appendix F). This process estimates decreases in ^{14}C activity due to radioactive decay during transit between boreholes, which is converted into a transit time using the radioactive decay equation (Eq. 3-1). After determining the transit time between boreholes, linear groundwater velocities can be determined by dividing the distance between the boreholes by the transit time.

The variability in $\delta^{13}\text{C}$ values (Figure 3-12) suggests that groundwater in the Yucca Mountain area has interacted to differing degrees with carbonate rock, minerals, or with groundwater from the carbonate aquifer, and therefore requires different degrees of correction to account for the effects. This conclusion also is indicated by the differing degrees of agreement between the organic and inorganic ^{14}C activities (Figure 3-14) and by the relationship between ^{14}C activity versus $\delta^{13}\text{C}$ (Figure 3-15). The scatterplot indicates that perched water at Yucca Mountain, groundwater in the northern Yucca Mountain crest area (YM-CR boreholes), and groundwater beneath Fortymile Wash have the highest ^{14}C activities and lightest $\delta^{13}\text{C}$ values, whereas groundwater from the Timber Mountain area and from the carbonate aquifer in the Yucca Mountain southeast (YM-SE) group have the lowest ^{14}C activities and heaviest $\delta^{13}\text{C}$ values. Collectively, the data display a trend that can be interpreted in a number of ways. Calcite dissolution or mixing of local recharge with isotopic characteristics of perched water with groundwater from the carbonate aquifer or from Timber Mountain are possible explanations for the observed trend between $\delta^{13}\text{C}$ and ^{14}C . Both of these processes tend to introduce dissolved inorganic carbon with heavy $\delta^{13}\text{C}$ and little ^{14}C . This explanation assumes that points on the trend are of the same age, but that the water dissolved different amounts of calcite. However, the scatter of points about the trend could be due to inclusion of samples of different ages. The scatterplot (Figure 3-15) also substantiates the argument that groundwater in northernmost Yucca Mountain at some Yucca Mountain Crest (YM-CR) group boreholes originates primarily from local recharge rather than by the southerly flow of groundwater from Timber Mountain.

To provide an estimate of groundwater ages, corrected ^{14}C ages were calculated for locations within 18 km of the repository where groundwater had been identified from anomalously high $^{234}\text{U}/^{238}\text{U}$ ratios as having originated mostly from local recharge (Paces et al. 1998). Corrections were also made to the ^{14}C ages of groundwater from several locations for which $^{234}\text{U}/^{238}\text{U}$ activity ratios were not measured, but which may contain substantial fractions of local Yucca Mountain recharge based on proximity to groundwater with high $^{234}\text{U}/^{238}\text{U}$ activity ratios. Table 3-3 provides corrected and uncorrected ^{14}C ages for these locations.



00346DCd_023

Source: BSC 2003f, Figure 45.

NOTE: TM = Timber Mountain; FMW-N = Fortymile Wash–North; YM-CR = Yucca Mountain–Crest; YM-C = Yucca Mountain–Central; YM-SE = Yucca Mountain–Southeast; YM-S = Yucca Mountain–South; CF = Crater Flat; SCW = Solitario Canyon Wash

Figure 3-15. Correlation between ^{14}C and $\delta^{13}\text{C}$ in Perched Waters and Groundwater

Table 3-3. Chemistry and Ages of Groundwater from Seven Boreholes at Yucca Mountain

Borehole	$^{234}\text{U}/^{238}\text{U}$ Activity Ratio	^{14}C Activity (pmc)	DIC, as HCO_3 , (mg/L)	Corrected ^{14}C age (years)	Uncorrected ^{14}C age (years)
USW G-2	7 to 8	20.5	127.6	13,100	13,100
UE-25 WT#17	7 to 8	16.2	150.0	13,750 to 14,710	15,040
UE-25 WT#3	7 to 8	22.3	144.3	11,430 to 12,380	12,400
UE-25 WT#12	7 to 8	11.4	173.9	15,430 to 16,390	17,950
UE-25 c#3	7 to 9	15.7	140.2	14,570 to 15,300	15,300
UE-25 b#1 (Tcb) ^b	---	18.9	152.3	12,350 to 13,300	13,770
USW G-4	---	22.0	142.8	11,630 to 12,510	12,500

Source: BSC 2003f, Table 16.

NOTE: DIC = dissolved inorganic carbon,
pmc = percent modern carbon

3.2.3.5 Evaluation of Groundwater Velocities in the Yucca Mountain Region

Under ideal circumstances, the decrease in groundwater ^{14}C activities along a flow path can be used to calculate groundwater velocities. The calculation is straightforward when recharge occurs at a single location and the resulting groundwater does not receive additional recharge or mix with other groundwater downgradient from that location. In the Yucca Mountain area, the calculation of groundwater velocity based on ^{14}C activity is complicated by the possible presence of multiple, distributed recharge areas. If relatively young recharge were added along a flow path, the ^{14}C activity of the mixed groundwater would be higher, and the calculated transport times would be shorter, than would be the premixed groundwater without the downgradient recharge. Unfortunately, the chemical and isotopic characteristics of recharge from various areas at Yucca Mountain may not be sufficiently distinct to identify separate sources of local recharge in the groundwater. Conversely, if groundwater from the carbonate aquifer were to mix downgradient with Yucca Mountain recharge, the mixture would have a lower ^{14}C activity than the Yucca Mountain recharge component because of the high carbon alkalinity and low ^{14}C activity of the carbonate aquifer groundwater. However, the presence of groundwater from the carbonate aquifer in the mixture would be recognized because of the distinct chemical and isotopic composition of that groundwater compared with the recharge water, and the effect on the ^{14}C activity of the groundwater mixture could be calculated.

In this section, groundwater velocities are estimated along various flow path segments using the ^{14}C activities of the groundwater. Measured ^{14}C activities at the upgradient borehole defining the segment were adjusted to account for decreases in the ^{14}C activity resulting from water-rock interactions between boreholes (identified by PHREEQC mixing and chemical reaction models) (BSC 2003f). This adjustment to the initial ^{14}C activity is necessary to distinguish between the decrease in ^{14}C activity caused by water-rock interaction and the decrease in ^{14}C activity due to transit time between boreholes. After determining the transit time between boreholes, linear groundwater velocities were determined by dividing the distance between the boreholes by the transit time. Groundwater velocities were calculated for several possible flow paths south of the repository, as described below.

Flow Path Segment UE-25 WT#3 to NC-EWDP-19D–PHREEQC inverse models (BSC 2003f, Section 6.7.8) indicate that groundwater sampled from various zones in borehole NC-EWDP-19D could have evolved from groundwater at borehole UE-25 WT#3 (Figure 2-26). Transit times were calculated using the dissolved inorganic carbon values of groundwater at borehole UE-25 WT#3 and PHREEQC estimates of the carbon dissolved by this groundwater as it moves toward various zones at borehole NC-EWDP-19D. Groundwater in the composite borehole and alluvial groundwater require approximately 1,000 to 2,000 years to travel the approximately 15-km distance between boreholes. This equates to linear groundwater velocities of approximately 7.5 to 15 m/year. Groundwater in the deeper alluvial zones (Zone 3 [145.6 to 206.0 m] and Zone 4 [220.2 to 242.4 m]) requires approximately 1,500 to 3,000 years, and thus travels at a linear groundwater velocity of 5 to 10 m/year. In contrast, transit times calculated for groundwater from shallow Zone 1 (125.9 to 131.4 m) and Zone 2 (151.8 to 157.3 m) have transit times that range from 0 to about 350 years. Using the upper age of 350 years, groundwater flow from borehole UE-25 WT#3 to Zones 1 and 2 in borehole NC-EWDP-19D is about 40 m/year. This higher velocity may indicate that some of the shallow groundwater at borehole UE-25 WT#3 moves along major faults like the Paintbrush Canyon fault or that groundwater is more representative of local recharge conditions.

For comparison, similar analyses in the volcanic tuff aquifers in the vicinity of Yucca Mountain have been conducted by other authors. White and Chuma (1987) estimated flow velocities between 3 and 30 m/year while Chapman et al. (1995) estimated flow velocities of between 1.9 and 2.4 m/year.

Flow path Segment USW WT-24 to UE-25 WT#3–Transit times were calculated using the dissolved inorganic carbon values of groundwater at borehole USW WT-24 and PHREEQC estimates of the carbon dissolved by this groundwater as it moves toward borehole UE-25 WT#3. The transit time estimate based on the differences in dissolved inorganic carbon of groundwater at these boreholes is 216 years. This estimate of transit time and a linear distance between the boreholes of 10 km, results in a linear groundwater velocity of 46 m/year.

3.2.3.6 Summary of Interpretations of Carbon Isotope Observations

Although uncertainty and variability exists in the ^{14}C and $\delta^{13}\text{C}$ observations, they generally indicate advective transport times of unretarded species that range from a few hundred to a few thousand years along likely flow paths within the tuff and alluvium aquifers to a downgradient point (NC-EWDP-19D) close to the compliance boundary. These advective travel times are similar to those that result from the saturated zone flow and transport model, which is presented in Section 3.4.

3.3 RADIONUCLIDE SORPTION PROCESSES

Sorption reactions are chemical reactions that involve the attachment of dissolved chemical constituents to solid surfaces. Although these reactions can be complex, they typically are represented in transport calculations by a constant, the sorption coefficient (K_d). In the literature, the sorption coefficient is often referred to as the distribution coefficient. The sorptive properties of the tuff and alluvial aquifers have been studied in laboratory and in situ tests.

In addition to sorption processes, radionuclide migration can also be affected by precipitation reactions caused by different geochemical conditions along the groundwater flow path. The most important control on precipitation reactions in the saturated zone at Yucca Mountain is the effect that reducing conditions could have on the behavior of several redox-sensitive radionuclides (e.g., technetium).

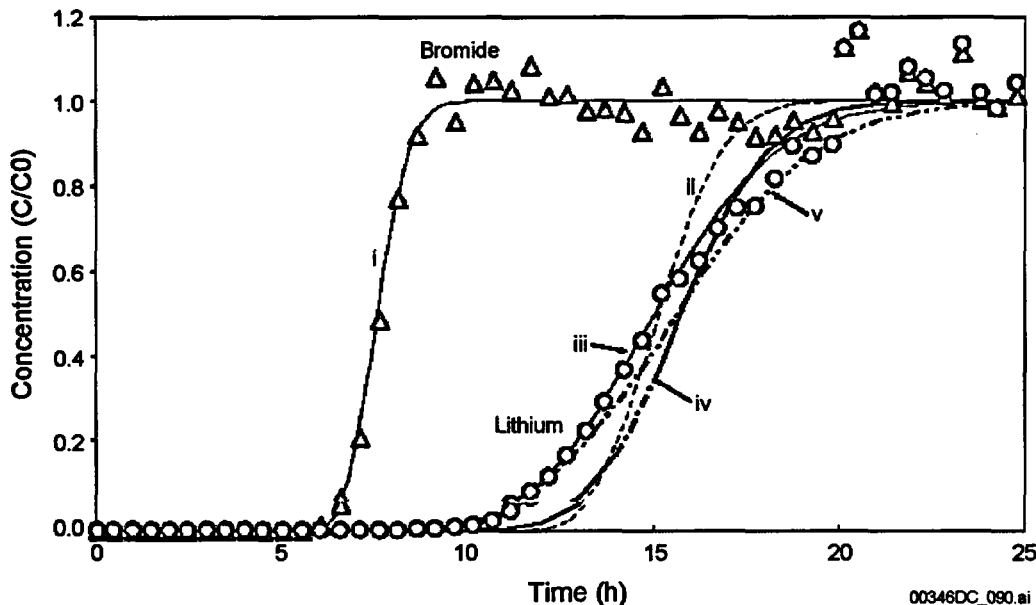
Reducing conditions have been observed in the groundwater of several boreholes in the vicinity of Yucca Mountain (Appendix L). A summary of this information is presented in Appendix K. In addition, there is a range of redox conditions in alluvial groundwater, as measured in groundwater pumped from Nye County boreholes. For example, groundwater in the central portion of the expected flow path (e.g., at boreholes NC-EWDP-19D and NC-EWDP-22S) generally has oxidizing conditions (with the exception of Zone 4), while groundwater to the east (e.g., NC-EWDP-5S) and west (e.g., NC-EWDP-1DX and NC-EWDP-3D) has reducing characteristics.

Although reducing conditions have been observed (see Appendix K), the groundwater chemistry along the likely flow paths generally is oxidizing. Because oxidizing conditions yield a more conservative transport behavior, the possible precipitation reactions have not been considered in postclosure performance assessment analyses.

3.3.1 Radionuclide Sorption on Fractured Tuff

Sorption reaction interactions potentially can occur on the surfaces of fractures and within the rock matrix of the fractured tuff. However, because of a lack of data and to be conservative, sorption on fracture surfaces is neglected, and only sorption within the matrix is included in the saturated zone transport model. In situ testing of sorptive characteristics has been performed at the C-Wells complex using analog tracers and in the laboratory using actual radionuclides of interest to repository performance at Yucca Mountain.

The C-Wells reactive tracer field experiments build on the detailed understanding of flow and advective transport characteristics obtained through a range of hydraulic and nonreactive tracer tests (Section 3.2.1). With an understanding of these processes at the C-Wells complex, interpretation of the reactive tracer test data can be accomplished using extrapolation to determine the sorption characteristics. The reactive tracer chosen as the analog was lithium. An example test conducted in the laboratory is represented in Figure 3-16. The range of laboratory-derived lithium sorption coefficients (K_{ds}) is between 0.084 to 0.32 ml/g (BSC 2003e, Table 6.3-11).



Source: BSC 2003e, Figure 6.3-60.

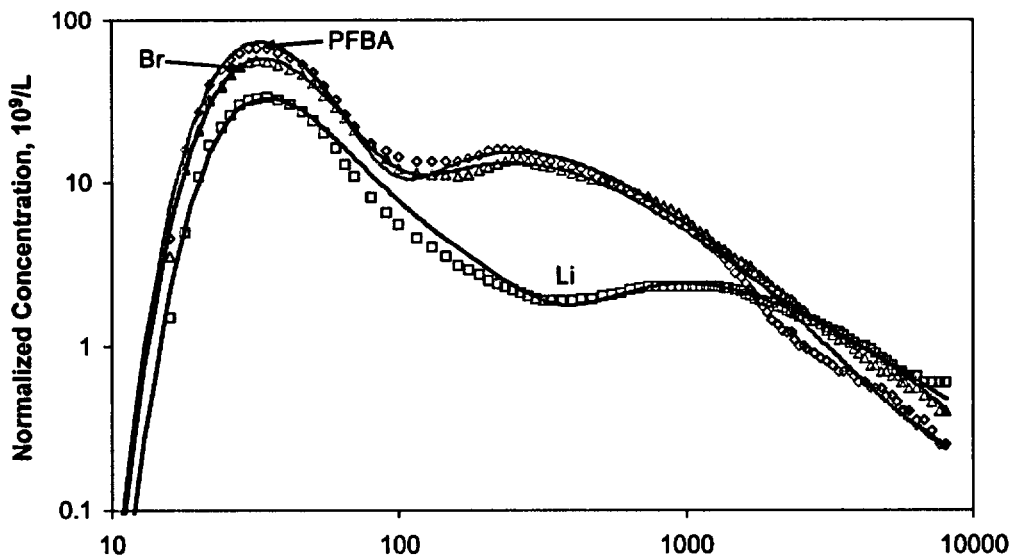
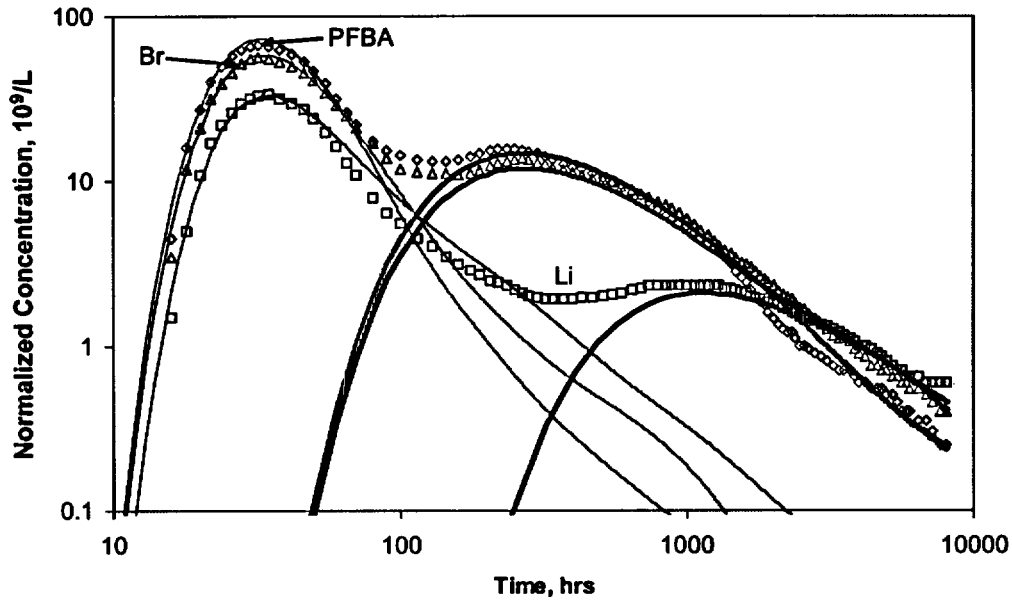
NOTES: The curves are numbered:

- (i) fit to bromide data with a Peclet number of 250
 - (ii) fit to lithium data assuming linear isotherm (see Appendix J) ($R_F = 2.0$) with equilibrium sorption
 - (iii) fit to lithium data assuming linear isotherm with a forward rate constant of 3.1/hr (and $R_F = 2.0$)
 - (iv) fit to lithium data assuming a Langmuir isotherm with equilibrium sorption
 - (v) fit to lithium data assuming a Langmuir isotherm with a forward rate constant of 3.2/hr.
- Langmuir isotherm parameters: $K_L = 0.0058 \text{ mL}/\mu\text{g}$ and $S_{max} = 105.8 \mu\text{g/g}$ (batch isotherm values obtained for lithium on central Bullfrog Tuff from UE-25 c#2).

Figure 3-16. Bromide and Lithium Breakthrough Curves and Comparison to Model Fits

The results of one of the multiple-well injection-withdrawal tests are illustrated in Figure 3-17. The interpretation of these test results was modeled using a matrix-diffusion model with the sorption coefficient of the matrix as an adjustable parameter (CRWMS M&O 2000a, Section 3.1.3.2). The model results are compared to field observations in Figure 3-17, and the model fit to the data agreed well with the laboratory sorption test data. Thus, in addition to confirming the sorption characteristics of the tuff aquifer materials, this match provides an additional degree of confidence in the matrix-diffusion model. The fact that the early breakthrough of lithium had the same timing as that of the nonsorbing tracers, but with a lower normalized peak concentration, is consistent with matrix diffusion followed by sorption in the matrix.

Lithium sorption parameters were deduced from the field tracer tests. In these tests, lithium sorption always was approximately equal to or greater than the sorption measured in the laboratory (CRWMS M&O 2000a, Table 3-4). Details of the methods used to obtain the field lithium sorption parameters and discussions of possible alternative interpretations of the lithium responses are provided by Reimus, Adams et al. (1999) and in *Saturated Zone In-Situ Testing* (BSC 2003e).



00348DC_058.psd

Source: BSC 2003e, Figure 6.3-28

NOTE: The upper plot shows individual fits to first and second tracer peaks (MULTRAN and RELAP, respectively). The lower plots show composite fits. For clarity, the data points shown are a subset of the actual data.

Figure 3-17. Comparison of Lithium Tracer Test Results and Model Predicted Results at the C-Wells Complex

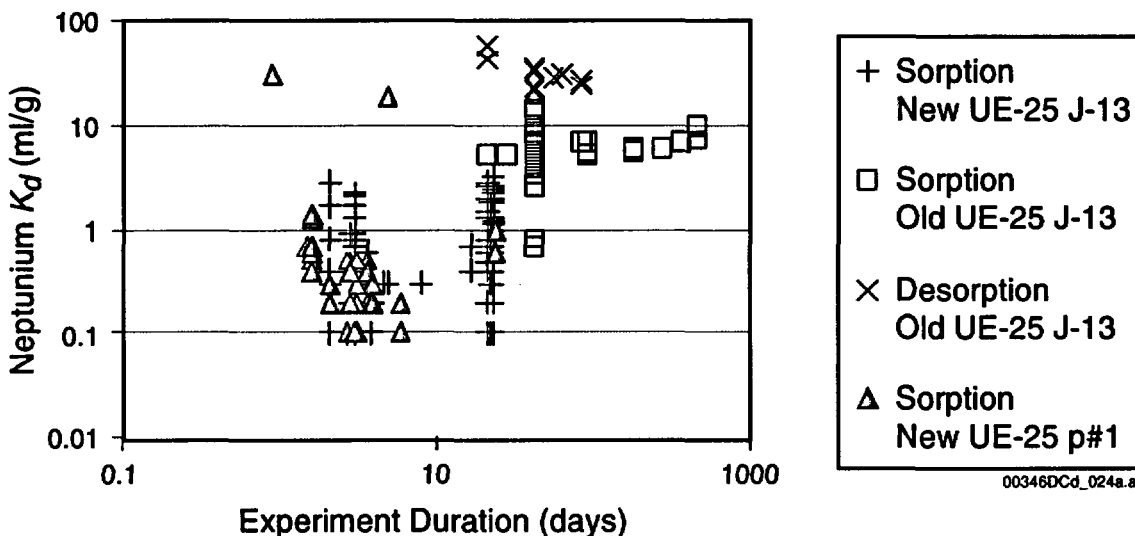
Experimental sorption coefficients (K_d values) were obtained using rock samples collected from the Topopah Spring welded and Calico Hills nonwelded hydrogeologic units at Busted Butte. To duplicate in situ conditions, the fine particles produced during sample crushing were not removed during the Busted Butte sorption study (BSC 2001e, Section 6.8.5.1.2.2), whereas fine materials were removed in the standard batch-sorption tests documented by Ding et al. (2003). Values for K_d could be influenced by small crushed-rock sizes used for sorption measurement, with the fine materials generating large K_d values. Sorption data determined during batch experiments are presented in Table 3-4.

The sorption data that were used as the basis of the distributions for neptunium, uranium, and plutonium (Table 3-4) are also presented in Figures 3-18 through 3-23. These data represent different types of experiments (sorption versus desorption), different water chemistries (derived from well UE-25 J-13 and borehole UE-25 p#1), different times when the experiment was performed ("old" are tests performed prior to 1990 and "new" are tests performed after 1990) and different durations of the experiment.

Table 3-4. Sorption-Coefficient Distributions for Saturated Zone Units from Laboratory Batch Tests

Parameter Name	Parameter Value Range (ml/g)	Distribution Type
Am K_d (volcanics)	1,000 - 10,000	Truncated normal
Am K_d (alluvium)	1,000 - 10,000	Truncated normal
Cs K_d (volcanics)	100 - 7500	Cumulative
Cs K_d (alluvium)	100 - 1000	Truncated normal
Np K_d (volcanics)	0.0 - 6.0	Cumulative
Np K_d (alluvium)	1.8 - 13	Cumulative
Pa K_d (volcanics)	1,000 - 10,000	Truncated normal
Pa K_d (alluvium)	1,000 - 10,000	Truncated normal
Pu K_d (volcanics)	10 - 300	Cumulative
Pu K_d (alluvium)	50 - 300	Beta
Ra K_d (volcanics)	100 - 1000	Uniform
Ra K_d (alluvium)	100 - 1000	Uniform
Sr K_d (volcanics)	20 - 400	Uniform
Sr K_d (alluvium)	20 - 400	Uniform
Th K_d (volcanics)	1,000 - 10,000	Truncated normal
Th K_d (alluvium)	1,000 - 10,000	Truncated normal
U K_d (volcanics)	0 - 20	Cumulative
U K_d (alluvium)	1.7 - 8.9	Cumulative
C/Tc/I K_d (volcanics, alluvium)	0.0	None

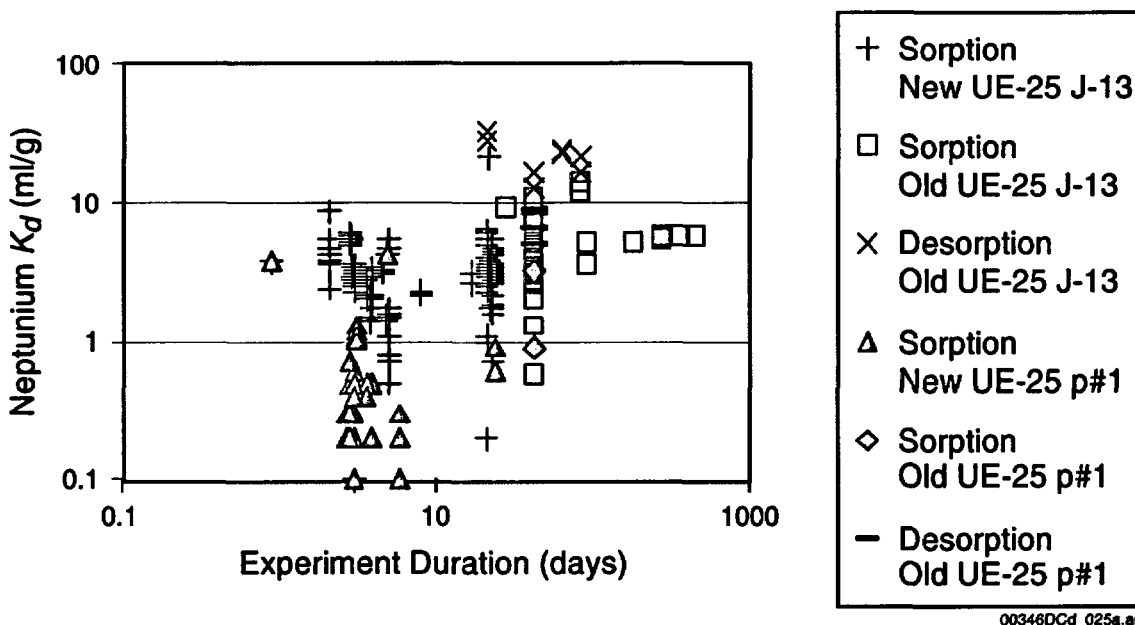
Source: Based on BSC 2003d, Table 4-3.



Source: BSC 2003a, Figure I-16.

NOTE: Experiments oversaturated with Np_2O_5 have been omitted.

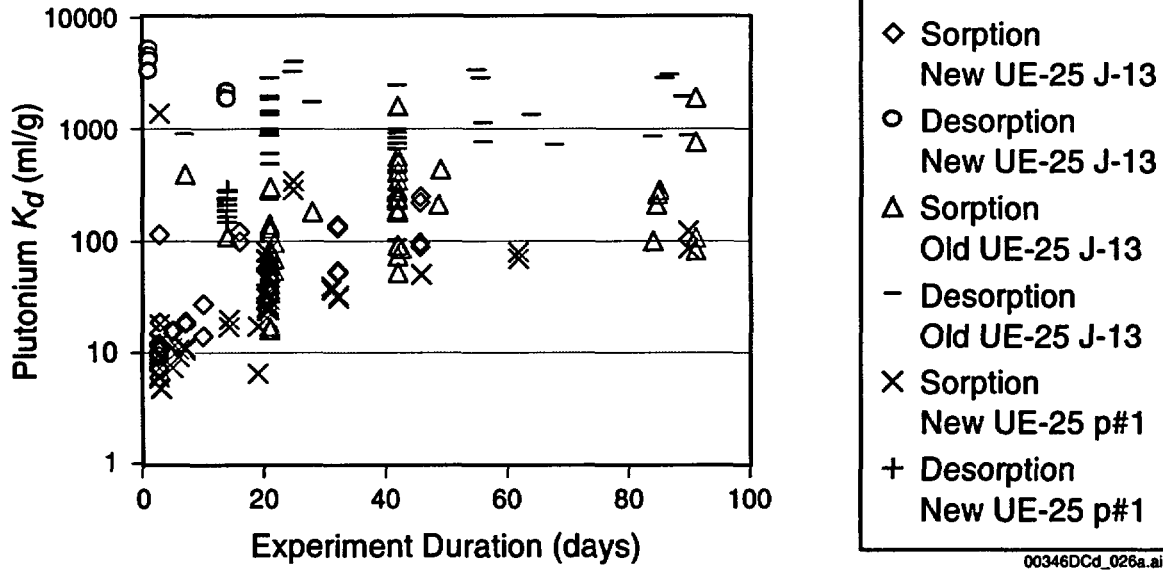
Figure 3-18. Neptunium Sorption Coefficients on Devitrified Tuff Versus Experiment Duration for Sorption and Desorption Experiments



Source: BSC 2003a, Figure I-20.

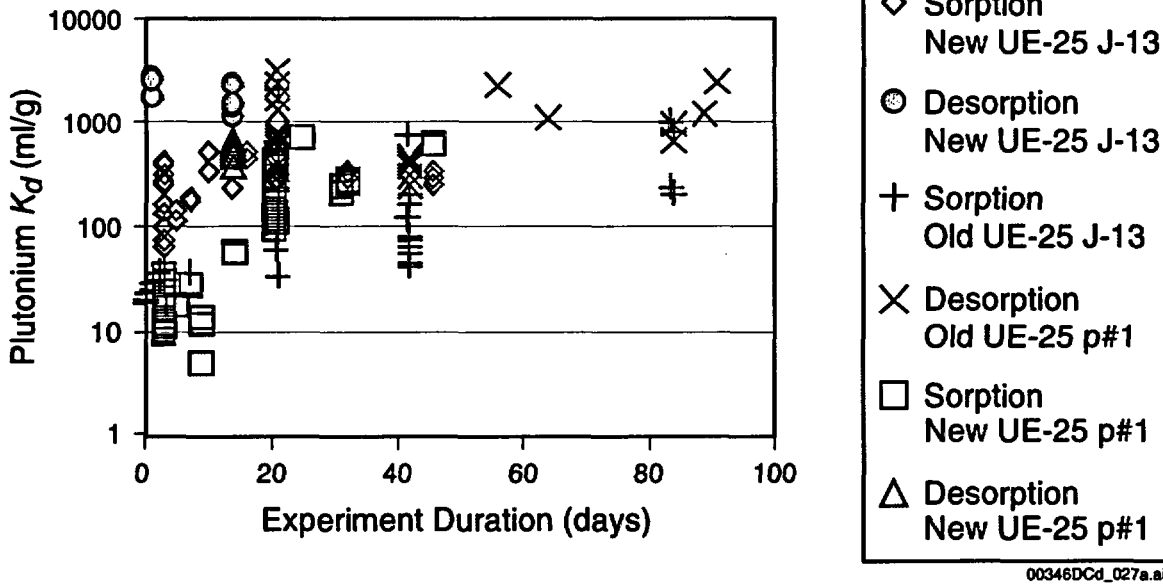
NOTE: Oversaturated experiments have been omitted.

Figure 3-19. Neptunium Sorption Coefficients on Zeolitic Tuff Versus Experiment Duration for Sorption and Desorption Experiments



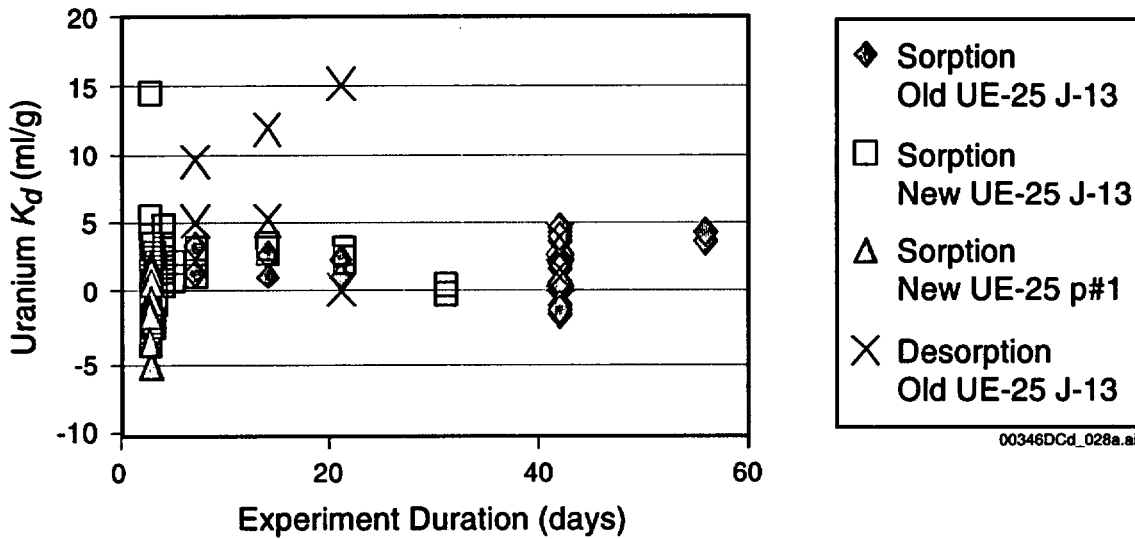
Source: BSC 2003a, Figure I-24.

Figure 3-20. Plutonium Sorption Coefficients on Devitrified Tuff Versus Experiment Duration for Sorption and Desorption Experiments



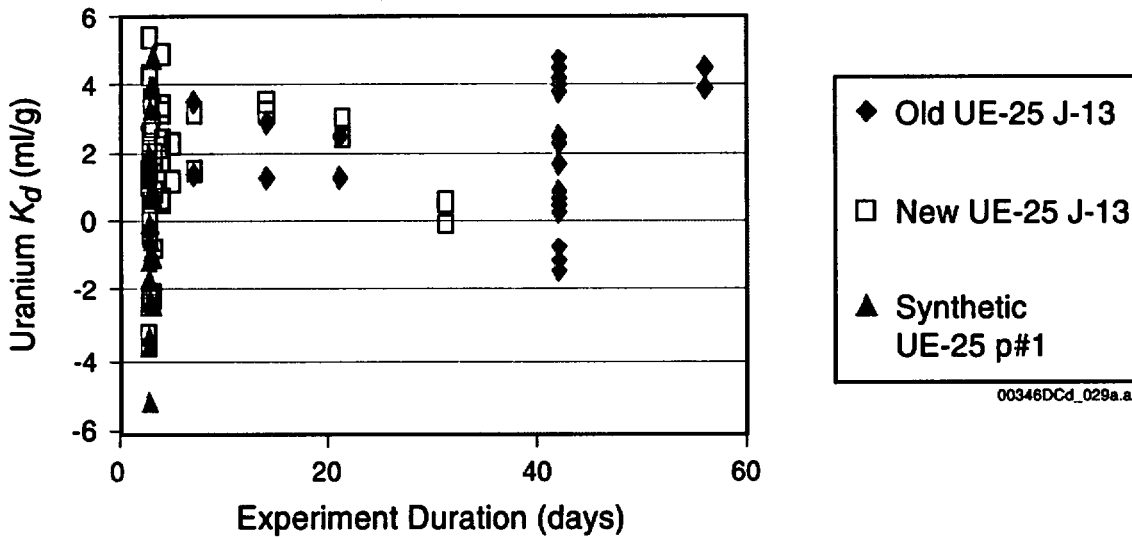
Source: BSC 2003a, Figure I-29.

Figure 3-21. Plutonium Sorption Coefficients on Zeolitic Tuff Versus Experiment Duration for Sorption and Desorption Experiments



Source: BSC 2003a, Figure I-48.

Figure 3-22. Uranium Sorption Coefficients on Devitrified Tuff Versus Experiment Duration for Sorption and Desorption Experiments



Source: BSC 2003a, Figure I-52.

Figure 3-23. Uranium Sorption Coefficients on Zeolitic Tuff as a Function of Experiment Duration

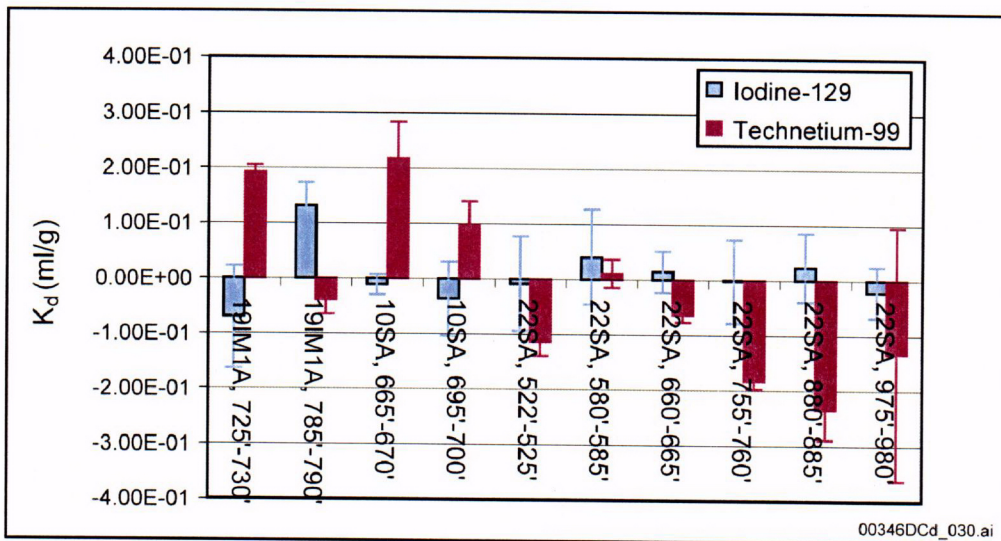
3.3.2 Radionuclide Sorption in the Alluvium

The migration behavior of sorbing radionuclides in the saturated alluvium south of Yucca Mountain has been studied in a series of laboratory-scale tests. The alluvium consists primarily of materials of volcanic origin similar to those found at Yucca Mountain (with some enrichment of clays and zeolites relative to common volcanic tuffs, plus secondary mineral coatings on the detritus).

Experiments conducted using alluvial materials focused on the transport characteristics of ^{129}I , ^{99}Tc , ^{237}Np , and ^{233}U . The first two were determined to be nonsorbing on tuff rocks, while the second two were moderately sorbed on tuff rocks. The goal of these experiments was to determine the sorption coefficient of the alluvial materials under conditions relevant to the field. To achieve these objectives, many batch sorption, batch desorption, and flow-through column experiments were carried out under ambient conditions to determine the sorption coefficients of these radionuclides between groundwater and alluvium from different boreholes.

The alluvium samples used in the experiments were obtained at various depths from three Nye County boreholes (NC-EWDP-19IM1A, NC-EWDP-10SA, and NC-EWDP-22SA). The alluvium samples used for batch experiments were dry sieved and size fractions of less than 75 μm , 75 to 500 μm , and 75 to 2,000 μm were used in different experiments. For column experiments, alluvium samples within a particle size range of 75 to 2,000 μm were wet sieved to remove fine particles that would clog the columns. Groundwater used in the experiments was obtained from borehole NC-EWDP-19D (Zones 1 and 4) and NC-EWDP-10SA. Mineral characterization of alluvium used in the experiments was determined by quantitative X-ray diffraction. Although the dominant minerals in the alluvium are quartz, feldspar, and plagioclase, considerable amounts of the sorbing minerals smectite (ranging from 3 to 8 percent) and clinoptilolite (ranging from 4 to 14 percent) were identified in the alluvial samples (see Appendix K).

The results of the batch sorption tests (Figure 3-24) indicate there is little sorption of ^{129}I and ^{99}Tc on the alluvium. The scatter of the results around $K_d = 0$ is representative of the degree of precision of the testing method. Negative K_d s are not physically possible.



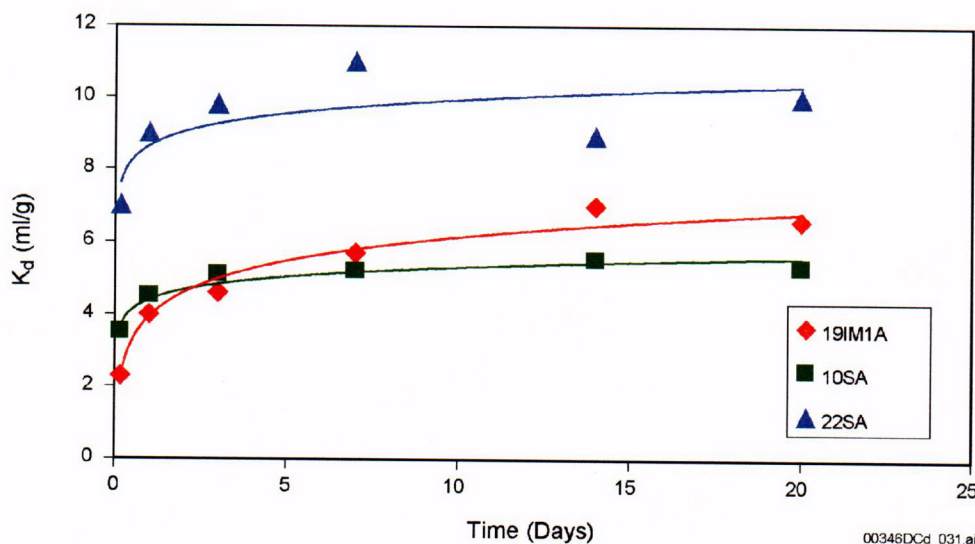
Source: Based on Ding et al. 2003, Figure 1.

NOTE: Borehole names refer to Nye County EWDP boreholes.

Figure 3-24. Sorption Coefficients of ¹²⁹I and ⁹⁹Tc in Alluvium

Figure 3-25 presents kinetic sorption of ²³³U in three alluvium samples. The results show that sorption of ²³³U onto alluvium is fast and that after one day of exposure, the amount of ²³³U adsorbed onto the alluvium changed little with time in all three tests. The higher K_d value from sample 22SA may be due to its higher smectite and clinoptilolite content (see Appendix K).

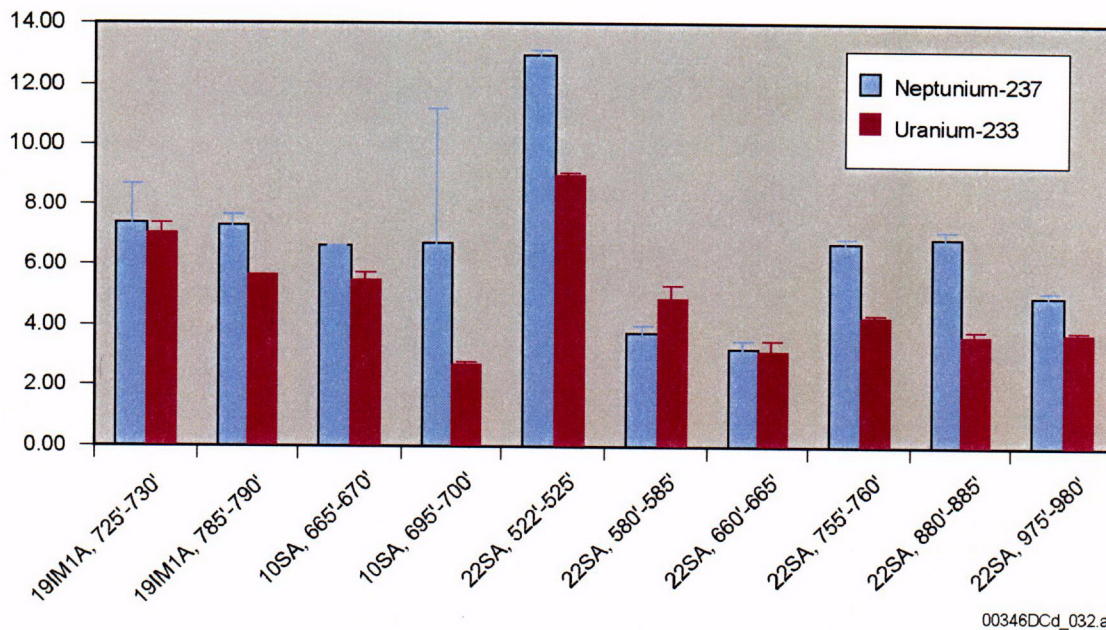
The experimentally determined K_d values of ²³⁷Np and ²³³U in alluvium are presented in Figure 3-26. The results suggest that sorption coefficients in the alluvium range from about 3 to 13 ml/g for ²³⁷Np, and from about 3 to 9 ml/g for ²³³U.



Source: DTNs: LA0302MD831341.003, LA0302MD831341.004.

NOTE: Borehole names refer to Nye County EWDP boreholes.

Figure 3-25. Sorption of ²³³U onto Alluvium as a Function of Time



Source: Ding 2003, Attachment B.

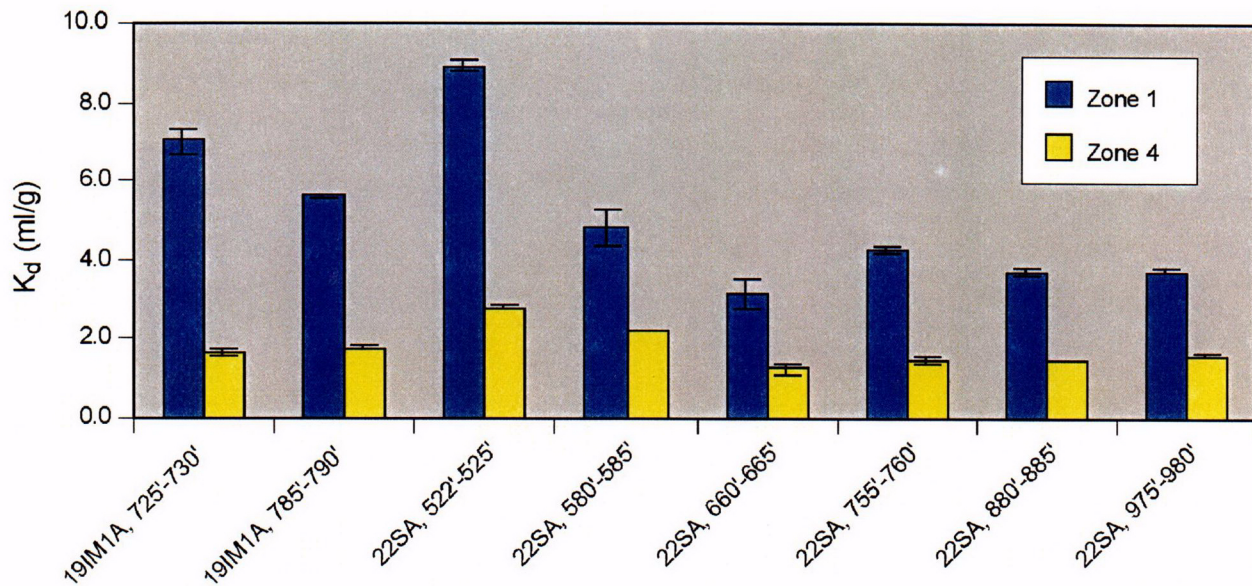
NOTE: Borehole names refer to Nye County EWDP boreholes.

Figure 3-26. Sorption Coefficients of ^{237}Np and ^{233}U in Alluvium

Tests were conducted to determine whether ^{233}U sorption behavior differs in groundwater from different zones in the same borehole (e.g., NC-EWDP-19D, Zone 1 and Zone 4). K_d values of ^{233}U measured in Zone 4 water were less than those from Zone 1 (Figure 3-27). The major differences between these two waters were the lower concentration of divalent cations and the slightly higher pH in Zone 4 than in Zone 1 (see Appendix K). These differences may result in greater complexation of ^{233}U to carbonate in Zone 4 water, as well as more sorption competition with divalent cations in Zone 1 water, both of which result in less sorption in Zone 4 water.

Experimentally determined K_d values for ^{237}Np range from about 4 to 500 ml/g (Figure 3-28). The particle size of the sample appears to affect the measured K_d value, as smaller particle sizes generally have larger K_d values.

Sorption experiments were performed on the same alluvial materials with groundwater from two boreholes, NC-EWDP-03S and NC-EWDP-19D (see Appendix K). The influence of groundwater from different boreholes on the sorption coefficients of ^{237}Np is negligible (Figure 3-29). Although these waters differed in major ion concentrations, they had similar pH values, and therefore similar ratios of carbonate and bicarbonate in solution. The results suggest that pH, and the corresponding carbonate concentration, may be more important than inorganic ion concentrations or the presence of trace amounts of drilling materials (which were found in NC-EWDP-03S water but not in NC-EWDP-19D water) in determining ^{237}Np K_d values.

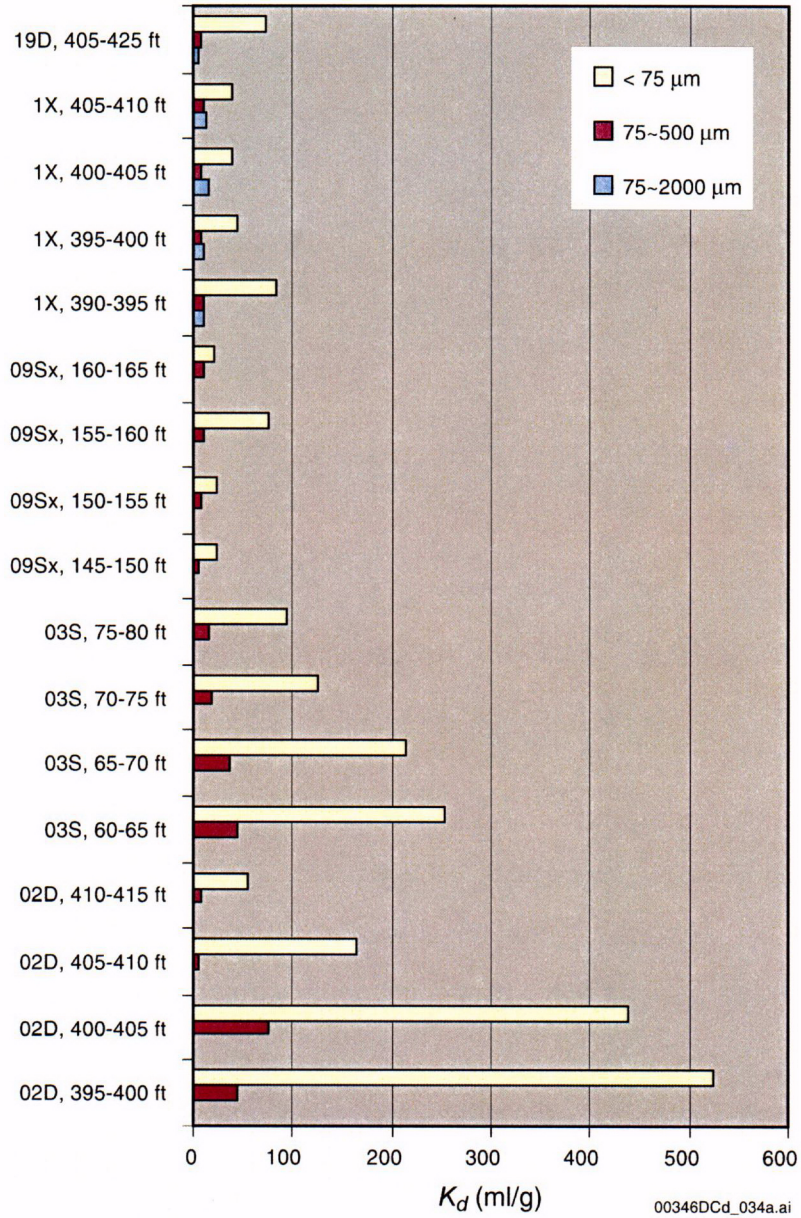


00346DCd_033.ai

Source: DTN: LA0302MD831341.004

NOTE: Borehole names refer to Nye County EWDP boreholes.

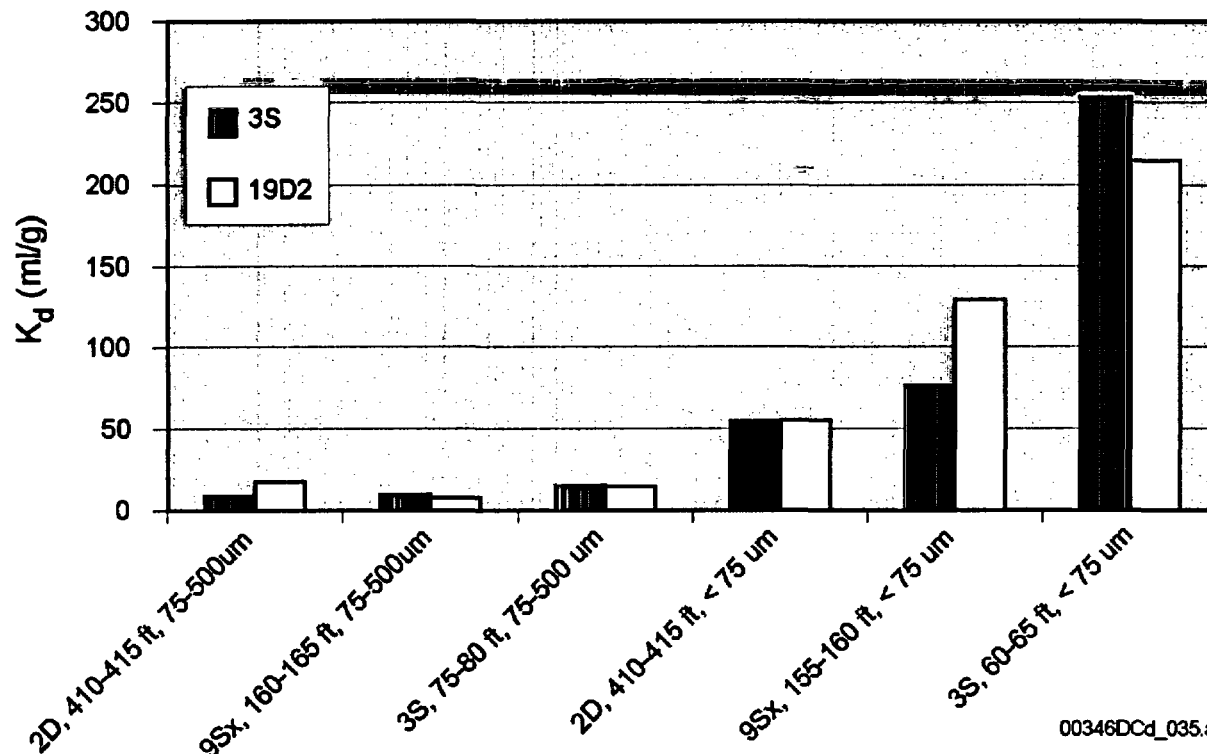
Figure 3-27. Sorption of ²³³U in NE-EWDP-19D Zone 1 and Zone 4 Waters



Source: Ding et al. 2003, Figure 2.

NOTE: Borehole names refer to Nye County EWDP boreholes.

Figure 3-28. Sorption Coefficients of ²³⁷Np(V) as a Function of Test Interval and Size Fraction Determined from Batch Experiments



00346DCd_035.ai

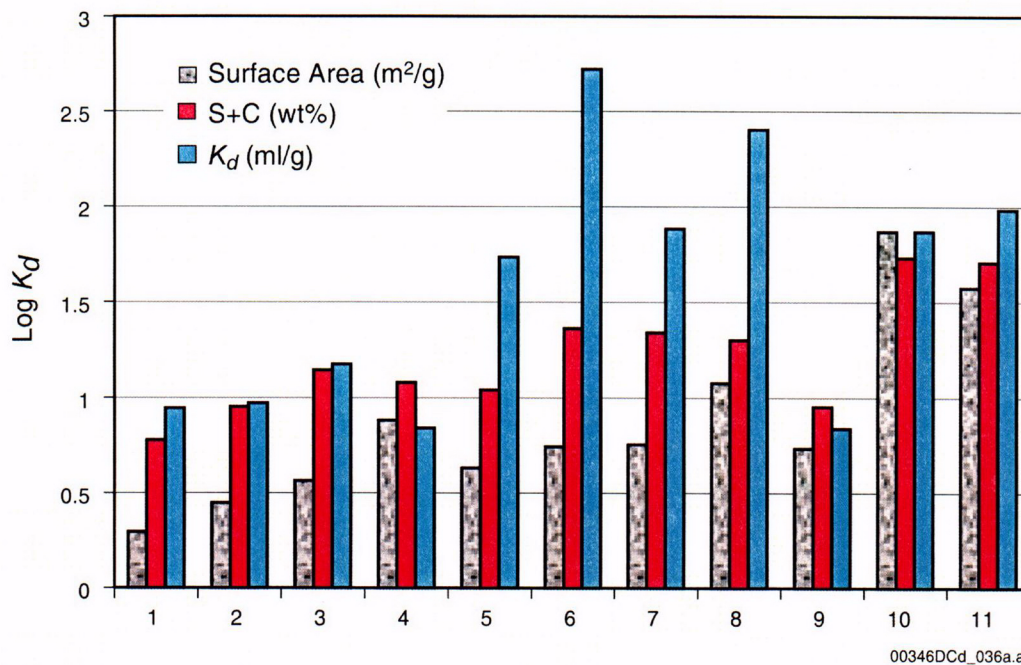
Source: Ding 2003, Attachments A and C.

NOTE: Borehole names refer to Nye County EWDP boreholes.

Figure 3-29. Sorption of Neptunium(V) on Alluvium

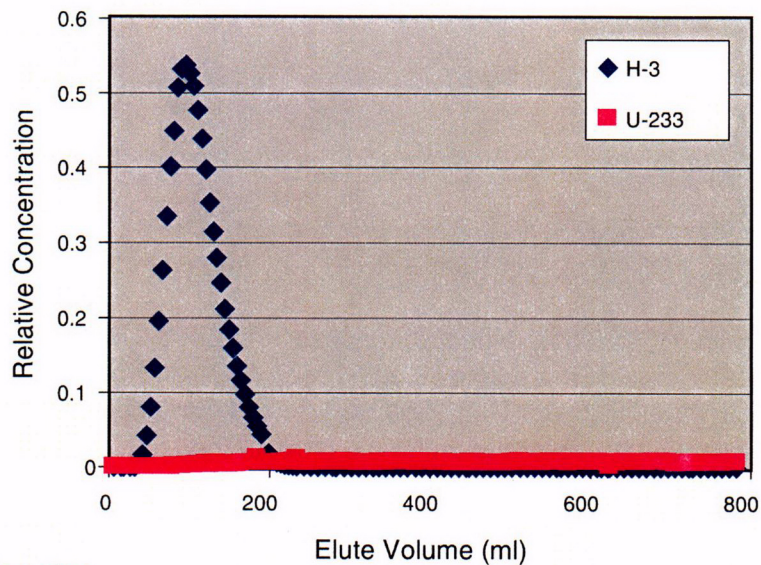
Sorption is generally dependent on the surface properties of the materials. In general, the larger the surface area of the sample, the larger K_d value under the same experimental conditions. Clay and zeolite minerals have larger surface areas than the primary minerals such as quartz and feldspar that compose the bulk of the alluvium. Therefore, alluvium, which contains large amounts of clay and zeolites, will generally have larger K_d values than the volcanic tuffs. Figure 3-30 presents ^{237}Np K_d values with respect to surface area and secondary minerals (the amount of smectite and clinoptilolite) content in alluviums. These results indicate that the correlation between sorption, surface area, and smectite plus clinoptilolite is as expected, with the exception that two high K_d samples do not have correspondingly high smectite and clinoptilolite content. These results suggest that trace amount of minerals such as amorphous iron and manganese oxides may affect the sorption of ^{237}Np in alluvium (see Appendix K). Additional studies of ^{237}Np sorption to vitric tuffs of Busted Butte indicated that sorption of radionuclides increases with increasing levels of smectite, iron oxide, and manganese oxide in the rock (BSC 2003a).

In addition to the batch experiments described above, column experiments were conducted. Figure 3-31 presents the results of a representative column test using ^{233}U compared to a nonsorbing tracer (tritium). Although the degree of ^{233}U sorption differs from column to column, the interpreted sorption coefficients are consistent with those observed in the batch experiments.



Source: Ding 2003, Attachments A and C.

Figure 3-30. Relationship Between Surface Area, the Amount of Smectite (S) and Clinoptilolite (C), and Measured K_d of $^{237}\text{Np(V)}$ of Alluvium



Source: Ding 2003.

NOTE: The total recovery of tritium is about 94 percent, and that of ^{233}U is about 10 percent. Flow rate is 10 ml/h.

Figure 3-31. Tritium and ^{233}U Breakthrough Curves for a Column Test

C14

In summary, ^{237}Np is sorptive on the porous materials of the alluvial aquifer, with sorption strongly dependent on the presence of clay minerals and iron and magnesium oxides that have large surface areas available for sorption.

3.3.3 Colloid-Facilitated Transport

Radionuclide transport may depend on colloids if the radionuclides sorb onto colloids. Colloid transport in the saturated zone is governed by several factors, including the percentage of colloids that irreversibly filter or attach to surfaces of subsurface materials, the rate at which radionuclides desorb from colloids, and the colloid concentrations that may compete with immobile surfaces for radionuclides. Analyses of colloid concentrations and size distributions in Yucca Mountain groundwater have not found high concentrations of colloids (BSC 2003b).

The filtering or attachment of colloids onto subsurface materials has been studied using polystyrene microsphere data from the C-Wells field tests to obtain conservative estimates of colloid attachment and detachment rates in fractured tuffs. Published data have been used to obtain bounding estimates of attachment and detachment rates in alluvium.

Laboratory experiments have been conducted to determine the magnitude and rates of sorption and desorption for strongly sorbing, long-lived radionuclides onto several different types of colloids that may be present in the near-field (iron oxides such as goethite and hematite that might result from degradation of waste package materials) or in the far-field (silica, montmorillonite clay) environment at Yucca Mountain (CRWMS M&O 2000b, Section 3.8). These studies used ^{239}Pu and ^{243}Am , with the plutonium being prepared in two different forms: colloidal plutonium(IV) and soluble plutonium(V). Also, water from Well UE-25 J-13 and a synthetic sodium-bicarbonate solution have been used in the experiments. Colloid concentrations were varied in some of the experiments to determine the effect of colloid concentration. Details of the experiment and summaries of the ^{239}Pu sorption and desorption rates onto the different colloids are provided in *Colloid-Associated Radionuclide Concentration Limits* (CRWMS M&O 2001). The results can be summarized as follows:

- The sorption of ^{239}Pu onto hematite, goethite, and montmorillonite colloids was strong and rapid, but the sorption of ^{239}Pu onto silica colloids was slower and less strong.
- The desorption rates of ^{239}Pu from hematite colloids were so slow that they are essentially impossible to measure after 150 days. Desorption from goethite and montmorillonite colloids also was slow, but faster than hematite. The desorption rates of ^{239}Pu from silica colloids was rapid relative to the other colloids.
- For a given form of ^{239}Pu , sorption generally was stronger, faster, and less reversible in the synthetic sodium-bicarbonate water than in natural Well UE-25 J-13 water. Apparently, the presence of other ions (probably calcium) in the natural water tend to suppress the sorption of ^{239}Pu .
- There was no clear trend of colloidal plutonium(IV) or soluble plutonium(V) being more strongly sorbed onto colloids. In general, it appeared that plutonium(V) was

sorbed slightly more to hematite and silica, while plutonium(IV) was sorbed slightly more to goethite and montmorillonite.

- The sorption of ^{239}Pu was greatest per unit mass of colloid at the lowest colloid concentrations, which implies that the most conservative K_d values for performance assessment will come from sorption data generated at low colloid concentrations.

The sorption of ^{243}Am onto hematite, montmorillonite, and silica colloids showed the same trends as ^{239}Pu sorption (i.e., for both ^{243}Am and ^{239}Pu , sorption onto hematite was stronger than sorption onto montmorillonite, and sorption onto montmorillonite was stronger than it was onto silica), and the magnitudes of sorption for the two radionuclides were similar for the different colloids.

This ongoing work indicates (BSC 2003b):

- Waste form colloids such as hematite pose the greatest risk for colloid-facilitated transport within the engineered barriers, but the importance of waste form colloids to saturated zone transport is mitigated by the fact that the colloids would have to migrate through the waste package, invert, and unsaturated zone before reaching the saturated zone.
- Natural clay colloids are likely to facilitate plutonium or americium transport more than silica colloids in the saturated zone.

Additional details of colloid-facilitated transport through the saturated zone are provided in the *Saturated Zone Colloid Transport* (BSC 2003b).

3.4 SITE-SCALE RADIONUCLIDE TRANSPORT MODEL

The site-scale saturated zone radionuclide transport model is designed to provide an analysis tool that facilitates understanding of solute transport in the aquifer beneath and downgradient from the repository. The transport model builds on the site-scale saturated zone flow model and the regional and site hydrogeologic and geochemical understanding obtained through field and laboratory studies. The data used in the development of the relevant transport parameters (e.g., sorption coefficient), submodel processes (e.g., advection and sorption), and site-scale model processes (e.g., flow paths and transit times) are based on laboratory testing, field tests, expert elicitation panel, and analog literature information. Transport parameters were derived consistent with NUREG-1563 (Kotra et al. 1996; see also Appendix H).

The principal output of the site-scale radionuclide transport model is the arrival time of important radionuclides at the point of compliance, which is located about 18 km south of Yucca Mountain. The arrival times are expressed as breakthrough curves of mass versus time. A representative plot of normalized mass arrival is illustrated in Figure 3-32. This figure illustrates mass breakthrough for an unretarded radionuclide species (e.g., technetium) and a moderately sorbing radionuclide (e.g., neptunium). For the retarded species, this figure illustrates the relative contribution of sorption in the alluvium versus sorption in the fractured tuff aquifers. For this representation, the total sorption is dominated by sorption that occurs on

the alluvial materials. This is the result of the combined effects of lower advective velocities in the alluvium (due to the effective porosity being greater than that in the fractured tuffs) and the higher sorption coefficient in the alluvium (Table 3-4).

Variability and uncertainty exist in the hydrogeologic properties and parameters that affect the prediction of radionuclide transport through the saturated zone. Variability of properties can occur over different spatial scales. For example, the effective porosity for developing advective transport velocity should be different at the scale of a core sample or in situ field test, as well as differing among hydrogeologic units. This difference was noted in the C-Wells test interpretation presented in Section 3.2.1.2. Knowing that the properties are variable allows for reducing the total variance of the property if the degree of spatial correlation of the property also is known.

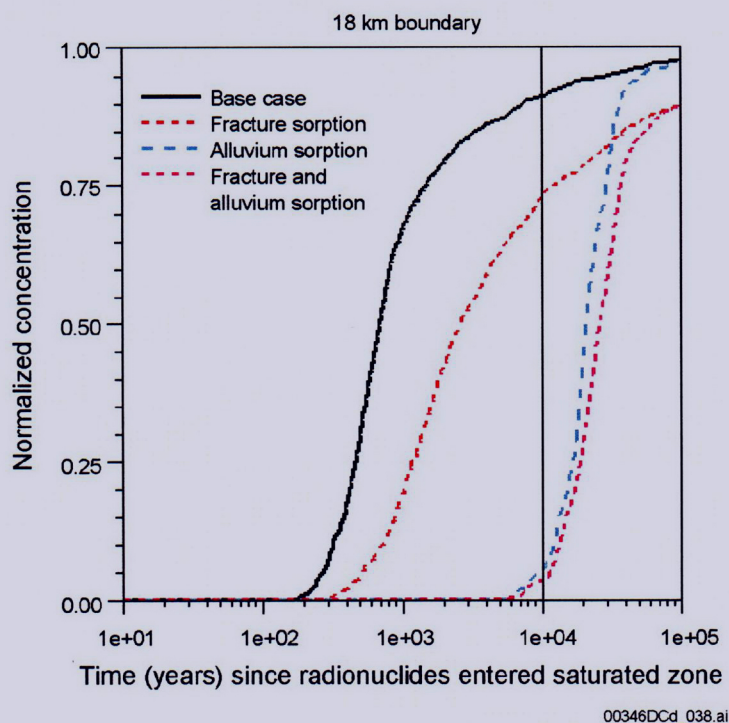
Rather than quantifying the degree of spatial correlation in flow and transport properties, the approach taken in the evaluation of saturated zone barrier performance was to first develop an integrated, self-consistent representation of the flow and transport processes that can be independently corroborated with other information (e.g., geochemistry and isotope information). After a model is developed, the approach consists of propagating uncertainty in all relevant flow and transport properties through the transport model to develop a distribution of possible breakthrough curves for different radionuclides. These breakthrough curves, all of which are equally likely based on current information, reflect the expected range of possible performance. In so doing, spatial variability has effectively been captured in the uncertainty reflected in the breakthrough curves. Additional discussions on the spatial variability of transport properties important to saturated zone performance are presented in Appendix I.

Uncertainty exists in many of the parameters that affect radionuclide transport through the tuff rocks and alluvium downgradient from Yucca Mountain. This uncertainty includes flow-related parameter uncertainty such as boundary condition fluxes from the regional model, hydraulic properties of the saturated tuff and alluvial aquifers, hydraulic potential and gradients, and anisotropy of the tuff aquifers. This uncertainty manifests itself in uncertainty in the flow path orientation, uncertainty in the percentage of the flow path from the repository to the compliance boundary that is in the tuff and alluvium, and uncertainty in the specific discharge within the saturated rocks and alluvium.

Uncertainty also exists in transport-related parameters such as the flowing interval spacing within the fractured tuff aquifers, the effective fracture porosity within the flowing intervals, the matrix diffusion between the fractures in the flowing intervals and the matrix between the flowing intervals, the effective dispersivity within the fractured tuff, the effective porosity of the porous alluvial materials, the sorption characteristics of the tuff matrix, the sorption characteristics of the alluvial materials, and the filtration and attachment-detachment characteristics of colloidally transported materials.

These uncertainties result in a range of projected advective-dispersive transport times for radionuclides. The transport model, considering the range of uncertainty, produces a range of possible breakthrough curves. The results for three representative radionuclides are illustrated in Figure 3-33. Figure 3-33a illustrates nonsorbing radionuclides (e.g., carbon, technetium, and iodine) with travel times ranging from several hundred and several thousand years. This is

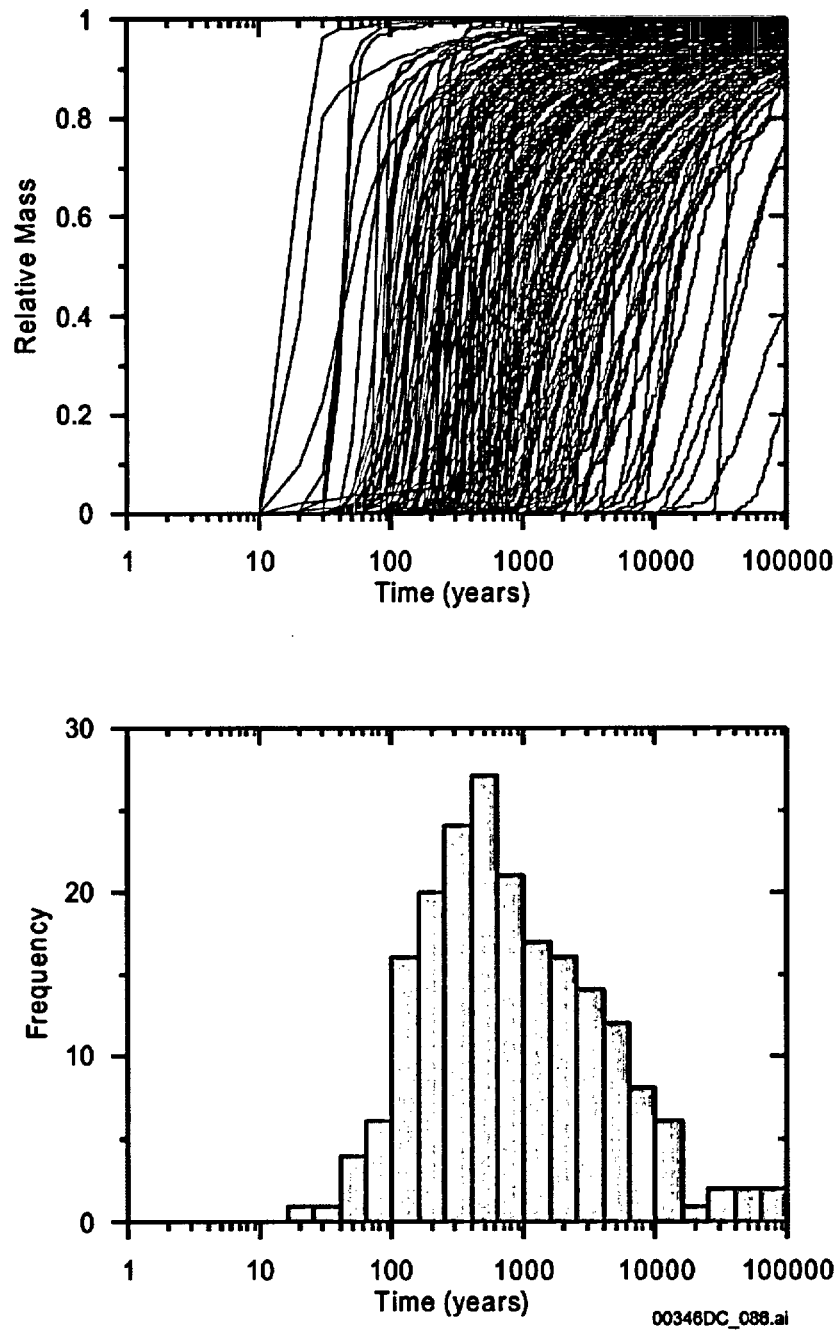
analogous to the distribution inferred from carbon isotope information presented in Section 3.2.3.4. For moderately sorbing radionuclides such as ^{237}Np (with K_d s in the range of 1 to 10 ml/g; Figure 3-33b), the travel times range from several thousand to over ten thousand years. For highly sorbing radionuclides (e.g., plutonium), travel times generally exceed 10,000 years (Figure 3-33c). For radionuclides in levels not yet achieved at the compliance point, transport times also exceed 10,000 years (Figure 3-34). These ranges in effective mass breakthrough reflect the combined effects of the uncertainties.



Source: BSC 2003a, Figure 6.7-1a.

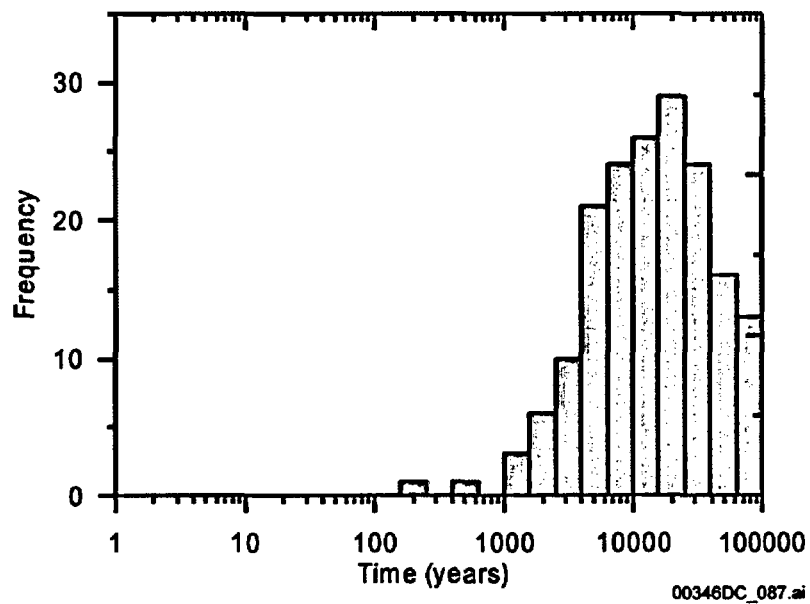
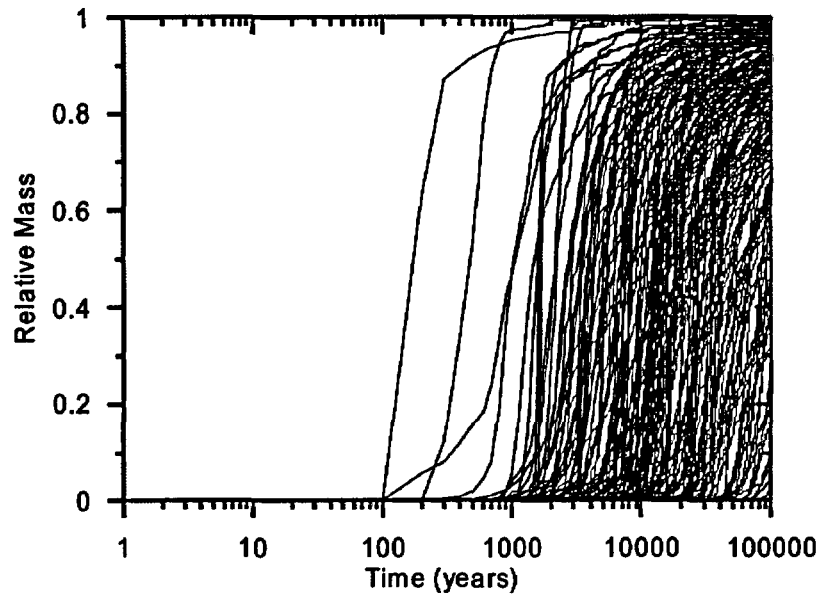
NOTE: Transport trajectories start in the saturated zone beneath the repository and migrate to the compliance point about 18-km south of the repository.

Figure 3-32. Predicted Breakthrough Curves



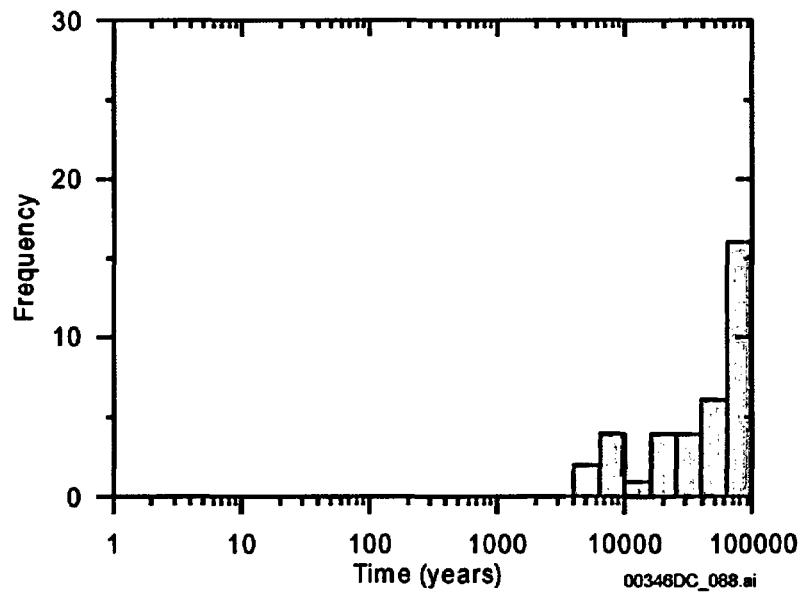
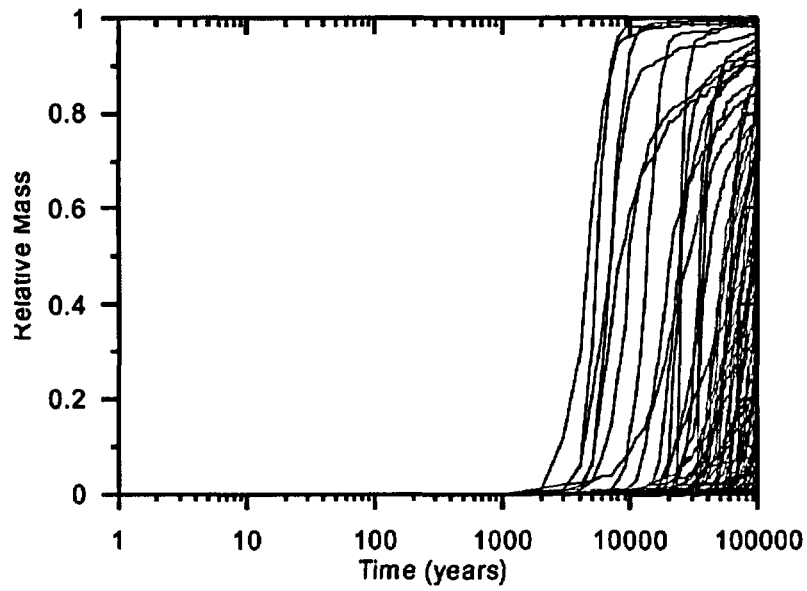
Source: BSC 2003d, Figure 6-28.

Figure 3-33a. Mass Breakthrough Curves (upper) and Median Transport Times (lower) for Carbon, Technetium, and Iodine at 18-km Distance



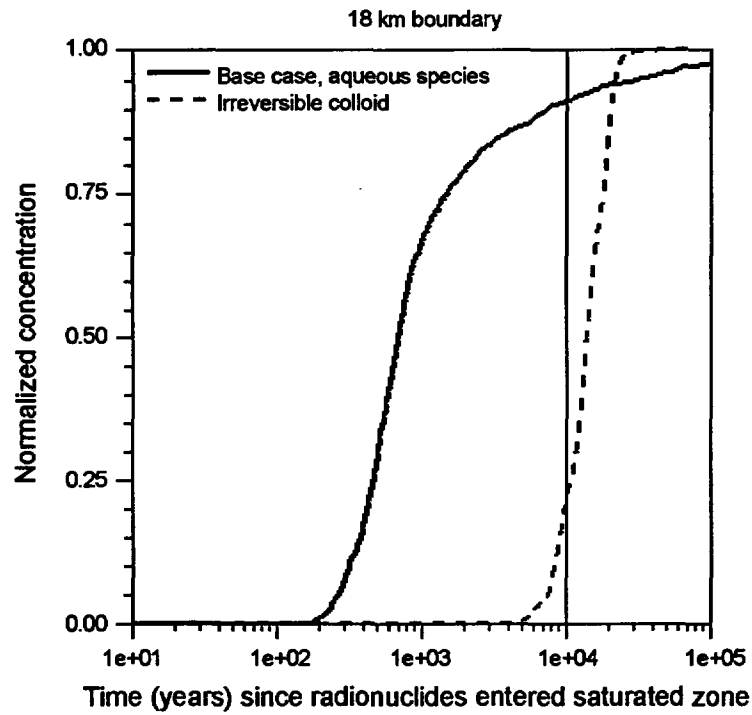
Source: BSC 2003d, Figure 6-32.

Figure 3-33b. Mass Breakthrough Curves (upper) and Median Transport Times (lower) for Neptunium at 18-km Distance



Source: BSC 2003d, Figure 6-31.

Figure 3-33c. Mass Breakthrough Curves (upper) and Median Transport Times (lower) for Plutonium at 18-km Distance



Source: BSC 2003a, Figure 6.7-5a.

NOTE: Base case refers to advective transport only.

Figure 3-34. Breakthrough Curves for the Base Case and Radionuclides Irreversibly Attached to Colloids at the 18-km Distance

INTENTIONALLY LEFT BLANK